



**HAL**  
open science

## Site Formation Histories and Context of Human Occupations at the Paleolithic Site of La Ferrassie (Dordogne, France)

Vera Aldeias, Dennis Sandgathe, Shannon J P Mcpherron, Laurent Bruxelles, Alain Turq, Paul Goldberg

► **To cite this version:**

Vera Aldeias, Dennis Sandgathe, Shannon J P Mcpherron, Laurent Bruxelles, Alain Turq, et al.. Site Formation Histories and Context of Human Occupations at the Paleolithic Site of La Ferrassie (Dordogne, France). *Journal of Paleolithic Archaeology*, 2023, 6 (30), 10.1007/s41982-023-00159-7. hal-04384610

**HAL Id: hal-04384610**

**<https://hal.science/hal-04384610>**

Submitted on 10 Jan 2024

**HAL** is a multi-disciplinary open access archive for the deposit and dissemination of scientific research documents, whether they are published or not. The documents may come from teaching and research institutions in France or abroad, or from public or private research centers.

L'archive ouverte pluridisciplinaire **HAL**, est destinée au dépôt et à la diffusion de documents scientifiques de niveau recherche, publiés ou non, émanant des établissements d'enseignement et de recherche français ou étrangers, des laboratoires publics ou privés.



Distributed under a Creative Commons Attribution 4.0 International License



# Site Formation Histories and Context of Human Occupations at the Paleolithic Site of La Ferrassie (Dordogne, France)

Vera Aldeias<sup>1</sup> · Dennis Sandgathe<sup>2</sup> · Shannon J. P. McPherron<sup>1,3</sup> · Laurent Bruxelles<sup>4</sup> · Alain Turq<sup>5,6</sup> · Paul Goldberg<sup>1,2,7,8</sup>

Accepted: 6 September 2023 / Published online: 18 October 2023  
© The Author(s) 2023

## Abstract

The Paleolithic site of La Ferrassie (Dordogne, France) has contributed significantly to the understanding of Middle and Upper Paleolithic technocomplexes, as well as Neanderthal skeletal morphology. Excavations at the site have spanned more than a century and uncovered rich archaeological assemblages associated with the Mousterian, Châtelperronian, Aurignacian and Gravettian technocomplexes. Renewed excavations exposed a sequence spanning both Middle and Upper Paleolithic occupations in the Western Sector and low-density Mousterian deposits and Châtelperronian in the Northern Sector. Here, we report on an extensive geoarchaeological study of deposits at the western end of the site to reconstruct and interpret both the depositional history of the sediments and associated human occupations in this poorly documented part of La Ferrassie. Our results point to the nature of the site as originally a karstic cave, with the Western Sector located in what would have been the cave's mouth. The stratigraphic sequence comprises first fluvial deposition (Phase I) followed by soliflucted deposits and accretion cones that emanate from an elevated platform situated several meters above the modern road next to the site (Phase II) and, finally, spatially restricted channeling (Phase III). Most archaeological assemblages are associated with Phase II and reflect an interplay between occupations directly in this area and bones and artifacts sliding down the slope from the upper platform. Unlike in the Western Sector, in the Northern Sector — situated along the north wall and several meters inside the footprint of the cave — cold features dominate the entirety of the sequence; we interpret these as being linked to microenvironments specific to this location of the karst rather than to general (external) climatic conditions. Relevant is the identification of patterned ground formation in this area, which can be clearly linked to the “monticule” features first reported by Capitan and Peyrony and erroneously interpreted as anthropogenic in origin. Our geoarchaeological results point to a large and complex karst system, with distinct depositional sources and often locally independent sedimentary histories throughout

---

Extended author information available on the last page of the article

its extent. These formation pathways have differently impacted the main occupation areas and resulted in distinct degrees of preservation of the archaeological assemblages throughout the different areas of the site.

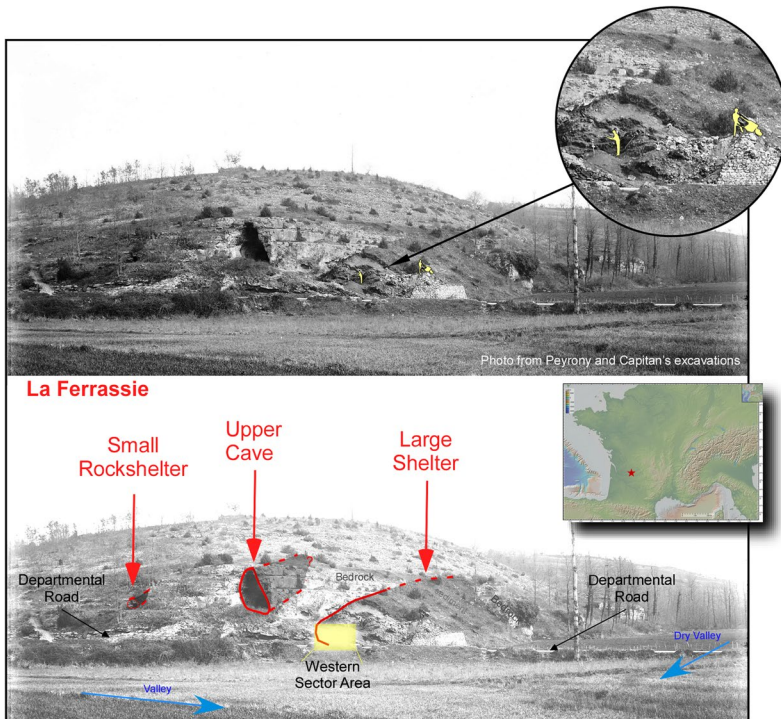
**Keywords** Site Formation Processes · Paleolithic Archaeology · Geoarchaeology · Neanderthals · Homo sapiens · Microstratigraphy

## Introduction

Understanding context is a fundamental aspect of archaeological research. Studies of site formation processes are thus crucial to support well-sustained inferences about past human behavior based on all forms of archaeologically related data (lithics, fauna, botanic, and equally important, the sediments). While this is true for any given archaeological site, it is particularly relevant for sites with a long history of research and for which artifactual assemblages have played a crucial role in archaeological systematics. One such “classic” Paleolithic context is the site of La Ferrassie (Dordogne, France).

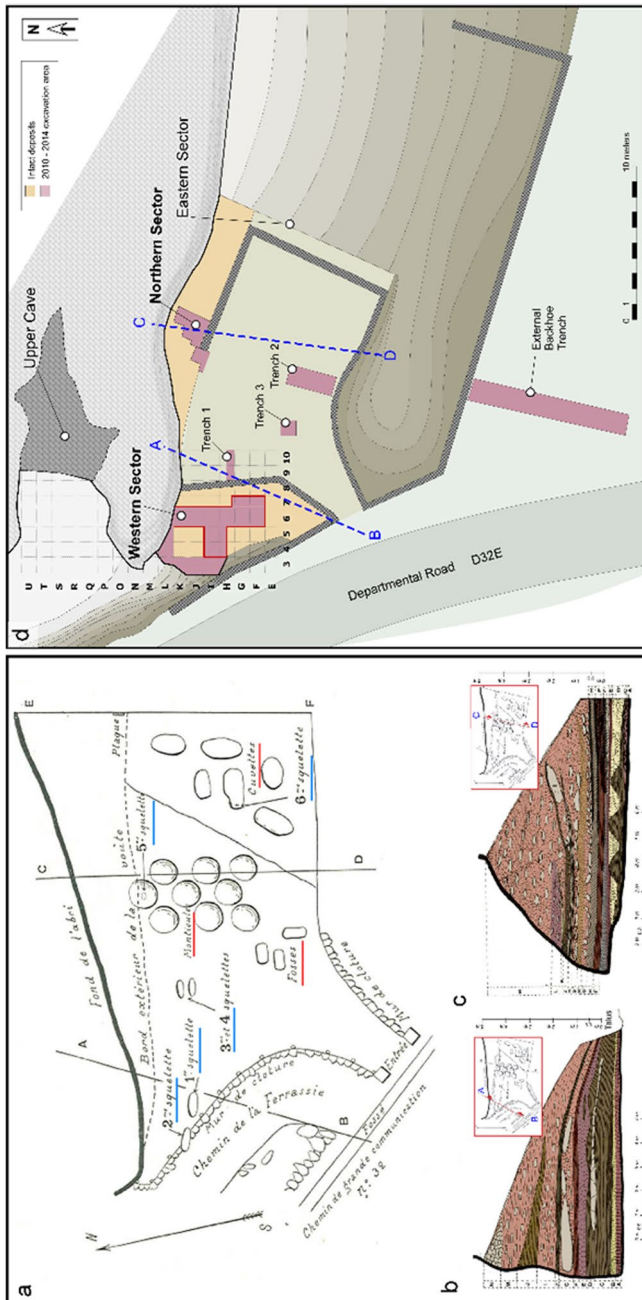
La Ferrassie is especially well known for a number of reasons: (a) it has yielded several Neanderthal skeletons, including two particularly well preserved adults and other partial skeletons (Breuil, 1921; Capitan & Peyrony, 1909a, 1912, 1921a; Delporte, 1984; Laville, 2007a); (b) it is the eponymous site for the ‘Ferrassie Moustérian’, a Middle Paleolithic lithic technocomplex variant initially characterized as rich in scrapers made on Levallois flakes (Dibble et al., 2018a, 2018b and references therein); and, (c) stages of the Upper Paleolithic Aurignacian technocomplex were originally based on the La Ferrassie sequence (Capitan & Peyrony, 1921b; Delporte et al., 1977; Peyrony, 1934). Over a century ago, the site was the focus of a number of excavations by Capitan and Peyrony (Figs. 1 and 2). Later studies in the 1970s led by Delporte focused particularly on the upper part of the sequence towards the Eastern and Northern sectors of the site (Fig. 2) and mainly investigated the Châtelperronian, Aurignacian, and Gravettian layers (Bertran et al., 2008a; Delporte, 1984; Texier, 2009). Between 2010 and 2014, a multidisciplinary research project uncovered unexcavated deposits in the Western and Northern Sectors of La Ferrassie (Turq et al., 2012). The Western Sector contains not only deposits associated with Upper Paleolithic and Châtelperronian assemblage types but also several underlying layers associated with the Middle Paleolithic. Importantly too, this area is adjacent to where Capitan and Peyrony began their excavations at the site over a century ago and where they found the two adult Neanderthal skeletons [(Capitan & Peyrony, 1909a, 1909b, 1911; Turq et al., 2012) — see Fig. 2]. Restricted excavations were also carried out in the Northern Sector where Delporte found a Neanderthal child, the LF 8 specimen (Balzeau et al., 2020; Delporte, 1984). This provided access to the broader depositional history and stratigraphic sequence of the site.

Here, we contribute new site formation data derived from our recent excavations, providing contextual information for the archaeological finds in the Western Sector, as well as correlations between this area and other previously excavated sectors, namely the



**Fig. 1** Top — Photograph of the sites of Ferrassie at the start of the excavations of Peyrony and Capitan (photograph from the Musée National de Préhistoire des Eyzies collection). For scale, people in the photograph are highlighted in yellow and shown in the inset close-up to the right; Bottom — Annotations showing the complex of sites associated with karstic hollows at La Ferrassie. The area of the current excavations (Western sector) is shown with the yellow rectangle in the lower image. Inset: Location of La Ferrassie (red star) within France (inset map generated with GeoMapApp)

Northern Sector. In this geoarchaeological study, we use archaeological, stratigraphic, fabric, geophysical and micromorphological data to reconstruct the nature of the karst system and to isolate the main depositional and post-depositional agents and processes. Formation aspects provide information on paleoclimatic conditions and help to constrain chronometric dates and to assess the degree of integrity of the archaeological assemblages. We show that the main part of the site, known as the ‘large shelter’ (*‘grand abri’*) of La Ferrassie is, in its origin, not a rock shelter but part of a cave system that has partially collapsed, and one that probably continues to the east of the current excavated areas. We also show that depositional mechanisms and sedimentary sources vary greatly across the different sectors of the site, with differences in depositional origins and distinct spatial timings of occupation resulting in a complex of distinct occupation areas rather than just one large archaeological site. Finally, our studies have also attested to periglacial conditions during the early Middle Paleolithic occupations with the development of cryogenic features — such as patterned ground — which helps explain some of the features originally described by Capitan and Peyrony and thought by them to be associated with some of the Neanderthal remains they uncovered.



**Fig. 2** Maps of the site of Ferrassie: (a) Map originally published by Peyrony (1934) showing the location of the Neanderthal skeletons identified during their excavations (blue lines), as well as mounds (“monticules”), pits (“fosses”) and basins (“cuvettes”) identified in the central and eastern areas of the site (red lines) north arrow indicates 1934 magnetic north; (b and c) Stratigraphic profiles and plan view from Capitan and Peyrony’s excavations. Modified from Laville (2007a) and based on drawings published in Peyrony (1934). The schematic cross section shown in (b) is the closest to our excavations in the Western Sector, whereas the schematic cross-section shown in (c) is closest to the deposits of the Northern Sector. Note the wavy lower Layer C and its correspondence with the location of what were called “monticules” in the plan view of Peyrony; (d) Plan view of the site as it is today, with the location of the areas excavated during the 2010–2014 fieldwork, including the test trenches (see SI for more info). The lines in blue mark the approximate location of the profiles shown in (b) and (c). North arrow in figure d indicates grid north; magnetic north is shown in a

## The Site of La Ferrassie

### General Geomorphological History

The site of La Ferrassie is located in the Périgord Noir, on the northeastern edge of the Mesozoic carbonate platform of the Aquitaine Basin (Karnay et al., 1999). The rocks are part of a thick sequence of Late Cretaceous carbonates that lie unconformably on Upper Jurassic limestones. At the end of the Late Cretaceous, the sea receded, and the region was subject to continental evolution and processes. Thus, after an extended period of weathering affecting the upper levels of Upper Cretaceous deposits, significant continental sedimentation took place by streams emanating from the Massif Central. These deposits constitute a thick cover that seals the limestones of the Upper Cretaceous and their *altérites* (residuum from extensive weathering of rocks).

It is only from the end of the Pliocene and especially from the beginning of the Quaternary Period that the incision of the hydrographic network began. It partly eroded the Tertiary detrital cover and then cut down into the Cretaceous limestones. The first karst circulations started to become organized from that moment. As river and tributary valleys developed, the tertiary cover was stripped, leaving exposed the *altérites* developed on the Cretaceous formations. With the gradual lowering of the base level during the entire Quaternary, the karstic underground drains were staggered, the older ones being gradually dismantled by the deepening and widening of the valleys. It is during these stages that the cavities that constitute the site of La Ferrassie were formed, along a valley of a small tributary of the Vézère River.

Three main archaeological loci are known at the site (Fig. 1): a small rock shelter located on a high platform to the north of the recent excavations, a small cave opening to the west (Upper Cave in Fig. 1) and, topographically below and to its south, ‘the large rock shelter’ (the ‘*grand abri*’) of La Ferrassie. In this paper, we focus mainly on the deposits of the so-called large rock shelter.

### A Brief History of Research

The construction of the Departmental road (D32E) that links Le Bugue to Rouffignac led to the identification of archaeological deposits in the large shelter area and to their subsequent excavations by Capitan and Peyrony, starting in 1907 and extending until 1922–1923 (Capitan & Peyrony, 1912; Delporte, 1984; Peyrony, 1934). Capitan and Peyrony undertook extensive excavations starting near the road in the west and progressively working towards the eastern areas of the large shelter (Fig. 2). Peyrony published a number of versions of his excavation profiles, with the cross-sections being very schematic (see analyses by Laville, 2007a for further details). These excavations yielded an important number of finds, including rich archaeological assemblages assigned to the Upper and Middle Paleolithic, as well as several Neanderthal skeletons (Peyrony, 1934). In addition, in the central area of the site, Capitan and Peyrony’s

excavations identified features described as “*monticules*” and “*cuvettes*” at the bottom of the sequence. At the base of one of these features, Peyrony found a Neanderthal skeleton, LF5 (see Laville, 2007b), and these *monticules* were then interpreted as anthropogenic features related to intentional interment of the individual.

Archaeological work at the site restarted in 1968 lead by Henri Delporte (Delporte, 1984). The excavation itself was carried out from 1968 to 1973 and focused on the two major profiles left by Peyrony: the very large north–south profile in the Eastern Sector that marked the end of Peyrony’s excavation and the east–west section running subparallel to the north wall of the large shelter, which we refer to here as the Northern Sector. The actual area of Delporte’s excavation was small relative to Peyrony’s:  $0.5 \times 12$  m in the Eastern Sector and  $1 \times 10$  m in the Northern Sector. At the end of the project, in the process of excavating along the north wall, Delporte uncovered a skeleton of a Neanderthal child (LF8) near the place where Peyrony found LF5 (a fetus) in 1920. The LF8 skeleton was recently reassessed by Gómez-Olivencia et al. (2015) and by Balzeau et al. (2020).

In terms of the geology, H. Laville and A. Tuffreau were responsible for the geology and sedimentology on Delporte’s project (Delporte, 1984). They identified 10 major sedimentary layers, starting at the base with Mousterian deposits (Layers M3 to M2a), Mousterian and Châtelperronian (L2B2), Châtelperronian and Aurignacian (L3a, L2c and L1b), followed by several Aurignacian layers, including Aurignacian I and II (layers L and L1a), Aurignacian II-II (K3 to I2), Aurignacian III (1 to H1), possible Aurignacian II-III and IV (F-G complex), final Aurignacian, the so-called Upper Perigordian with Font-Robert points (E and D), and Upper Perigordian with Noailles burins (C and B complex). In the Northern Sector, the stratigraphic sequence is shallower as it abuts the extending limestone wall.

Texier (Texier et al., 2006; Texier, 2009) and Bertran (Bertran, 2012; Bertran et al., 2008a) have since examined the exposed profiles left by Delporte’s excavations to investigate formation processes. This research indicates that slope processes, alongside roof fall contributions, are the main processes underlying the formation of the deposits exposed in the Eastern Sector. The effects of periglacial conditions with marked cold features were also discernable microscopically and were frequently observed. In the median part of the sequence (unit 2, corresponding to levels B and C of Delporte), colder depositional environments are associated with stone-banked solifluction lobes (Bertran et al., 2008a; Texier, 2009). Concerning sedimentary sources, Texier (2009) notes that the apex of the depositional talus migrated eastwards, with the lower levels (unit 3, corresponding to Levels L to I of Delporte) corresponding to a distal end of a talus whose maximum accretion was located roughly in the central area excavated by Peyrony (see below for more details). This talus apex shifts eastwards in the upper levels (upper part of unit 3 and unit 2, corresponding to levels G to B of Delporte). The basal Mousterian levels (M3 to M2a) were not available for study at the time of these studies.

## The 2010–2014 Excavations

In the mid-2000s, a thorough examination of the literature on the early work at the site led one of us (AT) to suspect that some Middle Paleolithic deposits had survived intact in the area of the site where Peyrony and Capitan first began digging in 1907 and where they uncovered the two adults Neandertals (LF1 and LF2). In 2009, limited backhoe testing confirmed this, and formal, multidisciplinary excavations were then carried out in this Western Sector area from 2010 to 2014 (Fig. 2).

*Western Sector:* The excavation methodology was based on that from previous excavations at several other Paleolithic sites and is described in more detail elsewhere (Dibble et al., 2018b). Over the 5 years of fieldwork, approximately 20 m<sup>2</sup> were excavated, and nine major layers were identified that span the late Middle and early Upper Paleolithic. These generally match Peyrony's (1934) sequence, though five Mousterian layers were recognized (to his four) along with four Upper Paleolithic layers (including one containing a Châtelperronian industry) (see Table 1). The sequence in the Western Sector has been dated by radiocarbon and luminescence techniques [see Table 1 and Frouin et al. (2017), Talamo et al. (2020) and Guérin et al. (2015)]. Briefly, at the base of the sequence, Layer 1 dates to late MIS 5 and Layer 2 to MIS 4. The majority of deposits (Layer 3, 4, 5, 6 and 7) are part of a single lithostratigraphic unit that was deposited at the end of MIS 4 and during MIS 3. The uppermost Layers, 8 and 9, have a very different lithostratigraphy and date to very late MIS 3.

The lithic assemblages in Layers 1 ( $n=526$  pieces) and 2 ( $n=841$  pieces) are characterized as Mousterian with small bifaces. The lithic assemblages in Layers 3 through 5b (Layer 3  $n=1660$  pieces, Layer 4  $n=1585$  pieces, Layer 5a  $n=648$  pieces, Layer 5b  $n=1256$  pieces) are all characterized as Mousterian with a relatively high Levallois component. In fact, it was Peyrony's corresponding layers at La Ferrassie that were used by François Bordes as the reference collection for defining his *Ferrassie Mousterian* facies. However, a recent re-examination of Peyrony's collection (Dibble et al., 2018a) has indicated a significant collection bias that would dramatically alter the percentage of retouched tools. As this was an important part of Bordes' definition of the Ferrassie Mousterian, the existence of this as discrete facies is in serious question (Dibble et al., 2018a, 2018b).

Layer 6 contains a Châtelperronian assemblage ( $n=2312$  pieces) and the lithic assemblage of Layer 7 (Layer 7a  $n=2810$  pieces, Layer 7b  $n=779$  pieces) is Aurignacian. While Upper Paleolithic in age, the lithic assemblage for Layer 8 is small and still under study. No Layer 9 deposits have survived in the Western Sector (if they did exist here, Peyrony removed them all), but there are still intact remnants on the terrace of the Upper Cave where they stratigraphically overlay Layer 8 which extends from the Western Sector up onto the terrace. As with Layer 8, the Layer 9 lithics are still under study.

The fauna from Middle Paleolithic Layers, 1 through 5, is generally consistent with temperate conditions: dominated by large bovids (bison [*Bison* sp.] and/or aurochs [*Bos primigenius*]). Red deer (*Cervus elaphus*) is also relatively abundant. Layer 4 has even more specifically warm/woodland indicators: roe deer (*Capreolus capreolus*) and wild boar (*Sus scrofa*). However, there are some indications of cooler



**Table 1** Stratigraphic sequence identified in the Western Sector, their correspondence with previous excavations with previous excavations by Captain and Peyrony, and age estimates

Stratigraphic units		Archaeological industry	Technique	Age (ka)	Reference
Phase	Layer				
IV	9	—	$^{14}\text{C}$	$27.1 \pm 150, 25.1 \pm 120$	Talamo et al., 2020
	8	—	$^{14}\text{C}$	$26.3 \pm 130, 27.2 \pm 150$	Talamo et al., 2020
III	7b	Aurignacian	$^{14}\text{C}$	$32.8 \pm 270, 33.7 \pm 290$	Talamo et al., 2020
	7a	Aurignacian	$^{14}\text{C}$	$33.1 \pm 260, 32.5 \pm 240, 32.6 \pm 230$	Talamo et al., 2020
	6	Châtelperronian	$^{14}\text{C}$	$37.4 \pm 390, 36.6 \pm 390, 39.0 \pm 510, 40.8 \pm 650, 40.9 \pm 500$	Talamo et al., 2020
II	5b	Mousterian with relatively high Levallois "Ferrassie Mousterian"	OSL	41.3–42.4	Guérin et al., 2015
			$^{14}\text{C}$	$42.2 \pm 2.9$	Guérin et al., 2015
	5a		$^{14}\text{C}$	$42.4 \pm 680, 42.2 \pm 660, 43.4 \pm 300, 42.0 \pm 310$	Talamo et al., 2020
			OSL	$45.8\text{--}47.3, 44.4\text{--}46.9, 44.5\text{--}47.2$	Guérin et al., 2015
	4		$^{14}\text{C}$	$43.1 \pm 2.6, 45.3 \pm 2.8$	Guérin et al., 2015
I	3		OSL	$41.7 \pm 310, 43.5 \pm 380, 42.4 \pm 330$	Talamo et al., 2020
			$^{14}\text{C}$	$43.1 \pm 2.6, 45.3 \pm 2.8$	Guérin et al., 2015
			$^{14}\text{C}$	$41.0 \pm 500, 40.0 \pm 440, 41.4 \pm 520, 40.2 \pm 590, 40.8 \pm 620, 39.2 \pm 520$	Talamo et al., 2020
			OSL	$44.4 \pm 2.6, 54.3 \pm 3.5, 44 \pm 3.0, 50 \pm 7.0$	Guérin et al., 2015; Frouin et al., 2017
			$^{14}\text{C}$	$45.3 \pm 820, 47.5 \pm 1060, 43.1 \pm 640$	Talamo et al., 2020
			OSL	$44.3 \pm 2.5, 51.5 \pm 2.7, 56.6 \pm 3.0, 63 \pm 7.0$	Guérin et al., 2015
			$^{14}\text{C}$	$44.3 \pm 2.5, 51.5 \pm 2.7, 56.6 \pm 3.0$	Guérin et al., 2015
			OSL	$63 \pm 7.0$	Frouin et al., 2017

**Table 1** (continued)

Stratigraphic units		Archaeological industry	Technique	Age (ka)	Reference
Phase	Layer				
II	Previous excavations <sup>1</sup>				
	B	Mousterian with bifaces	<sup>14</sup> C	>49	Talamo et al., 2020
I			OSL	62.5 ± 4.0, 74.2 ± 4.6	Guérin et al., 2015; Frouin et al., 2017
	Ib	Mousterian with bifaces	OSL	86.7 ± 7.2, 91.5 ± 8.8	Guérin et al., 2015; Frouin et al., 2017
	Ia	Sterile?			

**Table 2** Stratigraphic sequence identified in the Northern Sector, their correspondence with previous excavations and age estimations

Layer	Archaeological unit	Delporte layers	N lithics/bones	Technique	Age (ka)	Reference
E3	LAF9-1a	L2a	1/0			
E2	LAF8-1b	L2b1	0/0			
E1	LAF8-1c	L2b2	352/169	OSL (mdm)	43 ± 6	Balzeau et al., 2020
D	LAF8-2	L2bj?	232/63			
C	LAF8-3	M1?	8/2	OSL (mdm)	55 ± 3	Balzeau et al., 2020
B	LAF8-4	?	3/2	OSL (mdm)	67 ± 4	Balzeau et al., 2020
A	LAF8-5	M2?	42/6		60 ± 7	Balzeau et al., 2020

conditions including a steady, but low, presence of reindeer (*Rangifer tarandus*), some woolly rhinoceros (*Coelodonta antiquitatis*) elements in Layer 3, and some pronounced sedimentological indications of cooler conditions, especially in Layer 2 (see below).

For the Upper Paleolithic layers, despite a smaller faunal sample, there is a clear shift in climatic conditions beginning with Layer 6. These upper layers are dominated by reindeer, reflecting the colder and more open conditions associated with the onset of the Last Glacial Maximum.

*Northern Sector:* In 2014, limited work was also carried out in the Northern Sector. We undertook a cleaning of Delporte's original excavation profiles and carried out a small excavation (<2 square meters) directly adjacent to where Delporte discovered the remains of a Neanderthal skeleton LF8 (Delporte, 1984; Gómez-Olivencia et al., 2018). The goals were to try to establish a better understanding of the depositional context of the Neanderthal remains, retrieve any Neanderthal skeletal elements Delporte might have missed, and collect data on the archaeology and formation processes in this part of the site. One major issue with the Western Sector is that it is completely separated stratigraphically from the rest of the main cave site as these deposits were removed in the original Capitan and Peyrony excavations. However, the Northern Sector retains stratigraphic connection with the Eastern Sector and, though the archaeology here may not necessarily resemble that from other parts of the site, it did provide a window into the stratigraphy and site formation processes associated with the rest of the large shelter.

There is a considerably lower density of archaeological content in this area of the site, with only Layers D and E1 having more than 200 lithic finds (Table 2). A luminescence chronology is available for layers A to E1 (see Table 2).

*Test trenches:* In addition to the work carried out in the Northern and Western Sectors, three additional trenches were opened in the central area of the large shelter (see Fig. 2). The goal was to determine if any remnants of the lowermost layer of Capitan and Peyrony's Mousterian sequence had survived and whether they could

provide a direct, though limited, correlation with the stratigraphy of the Western Sector. Unfortunately, only pre-occupational deposits remain in the central part of the site and contain little or no archaeological material.

Also, a larger, fourth trench with a north–south orientation was opened at the south extremity of the site, adjacent to the road. This trench was intended to provide some indication of the nature of the deposits just outside the cave and of the topography of the bedrock as it sloped from the (estimated) location of the south wall of the cave into the valley to the south (see Fig. 2).

Detailed description of the stratigraphy of the trenches is presented in the Supplementary information and discussed below in the text where pertinent.

## Geoarchaeological Methods

### Lithostratigraphy

To reconstruct site formation histories, field investigations were based primarily on observations of the new and existing sedimentary profiles. Definitions of lithostratigraphic units in the field (which partially overlapped with archaeological associations) were based on their sedimentological attributes (color, grain-size, texture, sorting, compaction, sedimentary structures, thickness, etc.) and contacts between units. In the Western Sector, layers are labelled numerically from bottom to top, whereas in the Northern Sector layer designations are alphabetical to avoid confusion; they are also described from bottom to top. In addition to the archaeological deposits, field investigations also focused on the surroundings, including the description of the karst characteristics preserved in the Upper Cave, soils, and the limestone outcrops around the site.

### Archaeological Micromorphology

More in-depth analysis of site formation processes was done using archaeological micromorphological techniques. Archaeological micromorphology is an effective method for deconstructing site histories and formation processes, which represents the combined effects of geogenic, biogenic, and anthropogenic processes, as well as diagenesis (e.g., Aldeias et al., 2012; Courty et al., 1989; Goldberg, 1992; Karkanas & Goldberg, 2013, 2018; Karkanas et al., 2000, 2002; Mallol et al., 2013; Shahack-Gross et al., 2014; Weiner et al., 2002, 2007). Micromorphology involves the study of intact blocks of sediment (or soil) using petrographic thin sections (Courty et al., 1989; Macphail & Goldberg, 2017; Nicosia & Stoops, 2017; Stoops, 2021; Stoops et al., 2010, 2018) in which the microcontextual information is conserved (Goldberg & Berna, 2010).

Micromorphological samples were collected, either from exposed profiles or from columns left by the excavators. Samples were taken using two strategies: where the deposits were coherent, blocks were cut out with knife/trowel, wrapped with soft paper, and tightly bound with packaging tape; in the case of looser material, the

deposits were stabilized with plaster bandages before being removed (Goldberg & Macphail, 2003). At La Ferrassie and its surroundings, about 62 samples were collected and, in most cases, multiple thin sections were made from each (e.g., thin Sect. 101A, 101B...).

In the laboratory, sediment blocks were partially unwrapped, oven dried at 60° C for several days, and then impregnated with polyester resin diluted with styrene. After the resin gelled, samples were oven-cured overnight at 60 °C. They were then cut and trimmed with a rock saw to the appropriate dimension (either 7.5×5 or 9×6 cm). The smaller thin Sects. (7.5×5 cm), which comprise the majority, were produced by Spectrum Petrographics (Vancouver, WA, USA), and the larger ones (9×6 cm) were produced by Thomas Beckmann (Schwülper-Lagesbüttel, Germany). Thin sections were examined with stereo and petrographic microscopes in plane-polarized (PPL), cross-polarized (XPL) light, and ‘dark field’ illumination (see Goldberg & Aldeias, 2018) at magnifications varying from 8× to 200×. Nomenclature follows that of Courty et al. (1989) and Stoops (2021).

### Spectroscopy

The thin sections were analyzed with micro-Fourier transform infrared spectroscopy ( $\mu$ FTIR) using two types of equipment: a Thermo Scientific Nicolet iN10 MX microscope and an Agilent Technologies Cary 610 series microscope. In both cases, spectra were collected in attenuated total reflectance (ATR) mode using a germanium crystal at a 4  $\text{cm}^{-1}$  resolution with wavenumbers ranging between 4000 and 600  $\text{cm}^{-1}$  resolution. Each spectrum was the result of an average of 64 scans. The resulting spectra were compared with available libraries. High intensity burning associated with calcined bones at temperatures above 600–650° C (Stiner et al., 1995) were identified based on the presence of an absorbance band at 630  $\text{cm}^{-1}$  associated with the hydroxyl groups ( $\text{OH}^-$ ) and related to heat-induced changes (Figueiredo et al., 2010; Stiner et al., 1995; Thompson et al., 2009; Weiner, 2010).

### Fabric analyses: lithic orientation, edge damage, breakage, and small finds

Several measures of the excavated artifacts have also been shown to be good indicators of site formation processes (Goldberg et al., 2018). Here, we present data on artifact orientations, edge damage and breakage on stone artifacts, and artifact size classes. Some aspects of the La Ferrassie artifact orientations have been described and published previously McPherron (2018) and the methods covered by McPherron (2005, 2018).

Briefly, during excavation, artifacts larger than 2.5 cm in maximum dimension are piece-provenienced with a total station. Clearly elongated artifacts are targeted for orientation analysis and are recorded with two points, one at each extremity of the principal axis. A strict, numerical cut-off for what is elongated is not used. Subsequent lithic analysis on the Middle Paleolithic assemblages at La Ferrassie shows that for these artifacts, their elongation averages over 1.5 (McPherron, 2018). Orientations recorded this way can be divided into two components: a bearing and a

plunge. The bearing is the angle when the artifact is project onto an XY plane. A bearing of  $0^\circ$  is aligned with the positive Y axis of our excavation grid and angles increases clockwise. Without the plunge information, bearing angles have a periodicity of  $180^\circ$ . The plunge angle measures the slope of the longitudinal orientation of the artifact relative to the XY plane. When the artifact is coincident with the XY plane, it has a plunge angle of  $0^\circ$ . When it is perpendicular to the XY plane it has a plunge angle of  $90^\circ$ . Plunge angles have a periodicity of  $90^\circ$ . Bearing and plunge angles can be summarized and compared using circular statistics (see McPherron, 2005 and McPherron, 2018 and citations within).

Bearing and plunge angles can be considered together and graphically represented on Schmidt diagrams. Schmidt diagrams place either the higher or lower end of the artifact at the center of a sphere and then project onto the sphere's midplane the point where that artifact exits the lower or upper sphere respectively. Artifacts that lay flat plot near the edges of the resulting circular figure. Artifacts that are vertical plot near the center. Bearing angles, when considered this way, have a periodicity of  $360^\circ$ . Additionally, the 3D dimensional orientation of set of artifacts can be summarized using Eigen values and the results plotted on a Benn (1994) diagram by computing two ratios that summarize the magnitudes of the resulting set of three Eigen values. Benn diagrams are ternary with one pole representing artifacts randomly distributed on a plane, another representing artifacts clustering in a line, and the remaining pole represents artifacts that do not cluster in any dimension. Benn diagrams have been shown to be an effective means of characterizing orientations for understanding depositional processes (Lenoble & Bertran, 2004; McPherron, 2005) and substantial comparative data exists (e.g. Bertran et al., 2010; Larsen & Piotrowski, 2003; Lenoble & Bertran, 2004).

## Geophysics

When the excavations at La Ferrassie resumed, the paleogeography of the habitat in which the occupations took place remained to be clarified, especially since in the 2010s the hypothesis that the large shelter was in fact a cave had already been put forward (Texier, 2009). The purpose of the intervention by the company ArkoGéos was therefore to recognize the structure of the valleys near the deposit to provide details on the geomorphology of the limestone bedrock and its karstification (see Supplementary information).

The means implemented were measurements by electric panel (ABEM, SAS4000), which combines soundings and electric trails simultaneously permitting vertical and lateral exploration. In practice, a rectilinear network of regularly spaced electrodes is placed on the ground and all the possible quadrupoles are systematically measured. The electrodes, whose number varies between 12 and 128, have a regular spacing of between 1 and 5 m. The network of electrodes is controlled by a computer, which automatically varies the geometry of a quadrupole according to the desired depth of investigation. This quadrupole comprises 2 current injection electrodes (one of known intensity—I) and 2 electrodes for measuring the potential V induced in the ground by the injection of I.

The choice of devices was constrained by the physical limits of the area (parcel boundaries, obstacles, etc.) and the maximum depth of investigation desired. For the La Ferrassie 1 and 2 profiles, the inter-electrode spacing was 1.5 m, and 2.5 m for the La Ferrassie 3 and 4 profiles. The maximum theoretical investigation depths are approximately 16 m and 25 m respectively.

The device was the subject of several measurement protocols (Schlumberger, Dipole–dipole, Wenner  $\alpha$ ) to select the one best able to differentiate the different formations present on the site. After comparing the different pseudosections, the best precision/depth ratio is observed on the Schlumberger device, and this was then used on all the devices.

Specific results of the geophysical analysis relate to the larger geomorphological evolution of the region and will not be discussed in depth here but are summarized in the Supplementary Information.

## Results

### Sedimentary components

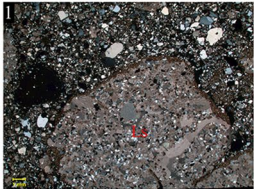
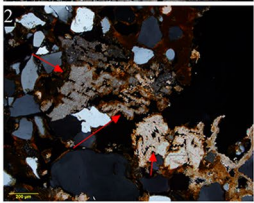

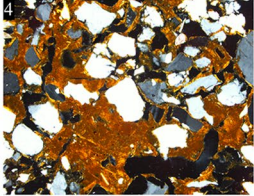
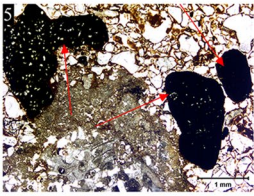
In thin section, a limited number of key sedimentary components make up the deposits at the site, and these can be assigned to geogenic, anthropogenic or biogenic origins. A detailed description of each of these components and their main occurrences within the lithostratigraphy are shown in Figs. 3 and 4 below.

*Geogenic input* components at the site are typical of cave sediments, namely quartz-rich, and in cases, calcite-rich (Layer 2) sands and silts, alongside limestone clasts deriving from the nearby breakdown of the limestone walls of the site. Components of more allochthonous origin are iron-rich rounded clasts (in Layer 1), which are present in the residual soils in the area and have been reworked into the site, mostly by colluviation.

*Biogenic inputs* in the Western Sector are mainly apatite-rich coprolites (typically sand- to a few mm-sized fragments). Their composition and microscopic features resemble those of hyaena coprolites (Horwitz & Goldberg, 1989). Interestingly, no other apparent field evidence was observed for hyaena activity at the site (e.g., in the zooarchaeological studies). On the other hand, bioturbation is present and mainly linked to root action and visible microscopically by the frequent presence of circular sand-sized calcareous root casts (rhizoliths), which occur particularly along the north wall. There, rhizolith formation represents the last post-depositional episode, as the rhizolith channels are not infilled by clay coatings or modified by other processes.

Other forms of physical modifications were noted: in rare instances, earthworm activity is expressed as biospheroids (Canti, 2017) that were identified in Layers 4 and 7. Large rodent burrows were rarely observed at the site. On the other hand, trampling is common and visible microscopically by the common presence of bones fractured in place, particularly, though not exclusively, in Layer 7.

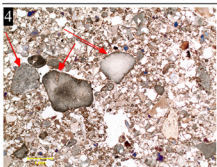
*Anthropogenic inputs* are abundant and expressed principally as sub-cm fragments of unburned, carbonized, and calcined bones, mainly from Layer 3 upwards.

	Component	Description
 	<p><b>Limestone (éboulis)</b> fragments resulting from the weathering and erosion of the walls and roof. Platy éboulis, ~10 cm in diameter, increase near the bedrock walls and the floor. Larger, dm-sized roof fall blocks during Layer 2 times and major roof fall events occur in association with Layer 4, and after the deposition of Layer 7.</p> <p>In thin section, ubiquitous angular to sub-rounded limestone clasts (cm- to silt-size). Rounded pebble-sized limestone are a minor component in Layers 5-7 and dominant in Layer 8.</p>	
	<p>The <b>sand- and silt-sized</b> fraction is dominated by quartz grains, though other minor quantities of siliciclastic minerals (feldspars and micas) occur in trace amounts. Also frequent are calcitic silts and sands. The latter are particularly frequent in association with Layer 2 deposits, though present in small percentages throughout all layers. Finely bedded quartz sands and silts are observed in Layer 1.</p>	
<p>Geogenic</p> 		
	<p><b>Clay fraction</b> occurs in small amounts in all samples, either as clay-rich domains (e.g., Layer 3), and red clay coatings (chitonic related distribution) or linking (gefuric related distribution) of the siliciclastic components (e.g., Layer 1 and deposits near the cave wall). Some degree of clay illuviation, with limpid or bedded clay coatings on voids is present in several thin sections.</p>	
	<p>Rounded, opaque <b>iron-rich clasts</b> and <b>pisolites</b> with silt-sized inclusions of quartz grains are present in Layer 1. These can be distributed within narrow (~10 cm wide) channels oriented roughly NW-SE. These materials are derived from the <i>sidérolithiques</i> soils in the site's surrounding and were reworked by water and gravity.</p>	

**Fig. 3** View in thin section of key geogenic components identified at the site, where ls = limestone

However, intact combustion features showing a common microstratigraphic sequence (e.g., ash overlying charcoal enriched deposits) were not observed. Nonetheless, discrete enriched concentrations of burned bone and char were observed — particularly in Layers 3 and 4 — that are interpreted as poorly preserved features related to combustion in some manner (Fig. 5). It is curious that the faunal analysts did not observe burning in the recovered bone. Interestingly, in the Western Sector sequence, charcoal fragments were identified only rarely and the percentages of burned flint are very low (0.7% for Layer 3; 1.1% for Layer 4; and 0.6% for Layer 5), whereas char fragments are relatively abundant.



	Component	Description
Anthropogenic and Biogenic		Abundant <b>bone</b> fragments, range from sand- to cm-size; the former are commonly rounded and distributed throughout the entire site. Several degrees of thermal alteration, with colors varying from white (calcined), black, and brown. Rarely, interconnected bone fragments indicative of trampling. No evidence for bone dissolution.
		Generally elongated, angular pieces of <b>chert</b> common from Layers 3 to 7, with rare fragments showing signs of spalling (red arrows). Correspond to lithic artifacts.
		Pieces of <b>char</b> (black, isotropic pieces with vesicular random porosity), presumably resulting from the combustion of animal fats. In (3) the char fragment displays silty capping. Only very few pieces of <b>charcoal</b> were observed in this section, and these seem to be even rarer in association with the Mousterian layers (Layer 3-6).
		Common phosphatic <b>coprolite</b> grains, with sizes ranging from coarse sand to granule; they are distributed throughout the sequence. Several of these are carnivore coprolites with their phosphatic-rich matrix and typical gas-derived porosity.

**Fig. 4** View in thin section of key anthropogenic and biogenic components identified at the site, where b = bone

## The Stratigraphic Sequence in the Western Sector

As mentioned above, we have identified nine main layers in the deposits excavated in the Western Sector (Fig. 6), and here, we present more in-depth sedimentological and microscopic descriptions.

**Layer 1. Field observations:** This is a somewhat complex deposit, and vertical and lateral lithological changes can be seen. With depth — and especially in sq. G6 — the limestone clasts are coarser (~10 cm) and blockier. In general terms, Layer 1 consists of red (2.5YR 4/6) poorly sorted sand with inclusions of some bone and numerous iron-rich clasts (up to 2–3 mm in size) derived from the *altérite* that occurs on the slopes above the site. Layer 1 was subdivided based on specific differences of lithology and texture (Fig. 7).

- The lower part, **Layer 1a**, (at least 35 to 25 cm thick, although the base is not exposed) is comprised of poorly sorted quartz sand with interstitial clay and iron coatings; it contains cm-sized platy limestone clasts, but larger and more equant ones increase towards the base and to the south. The color varies from red (2.5YR 4/6) at the bottom to yellowish red towards its top (5YR 5/8).

- Layer 1a is truncated by a channel-like feature, **Layer 1b**, which consists of limestone clasts (1 cm and 5–10 cm) and orange-red compact quartz sand with few calcite grains in a silty iron-rich matrix.

Layer 1a grades into a subdivision of Layer 1b (**Layer 1b1**), which is composed of red sand rich in platy limestone clasts, rounded pebbles, and is roughly 0 to 40 cm thick. In sq. H6 and I5, concentrations of iron-rich clasts locally occur in channels (~5 to 25 cm wide and a few cm deep) that are oriented NW–SE. In these areas, Layer 1b1 wedges out to the south as it is truncated by either Layer 1b2 or Layer 2.

Layer 1b1 grades into more homogenous yellowish red (5YR5/8) sand of **Layer 1b2** (~15 to 20 cm thick); locally, (sq. H-I-J7, J4 and J5) it exhibits thin laminations that cut into Layer 1a; in sq. J6 and J5, Layer 1b2 directly overlies Layer 1a. It is also truncated NW–SE by lobes of Layer 2 with a sharp contact.

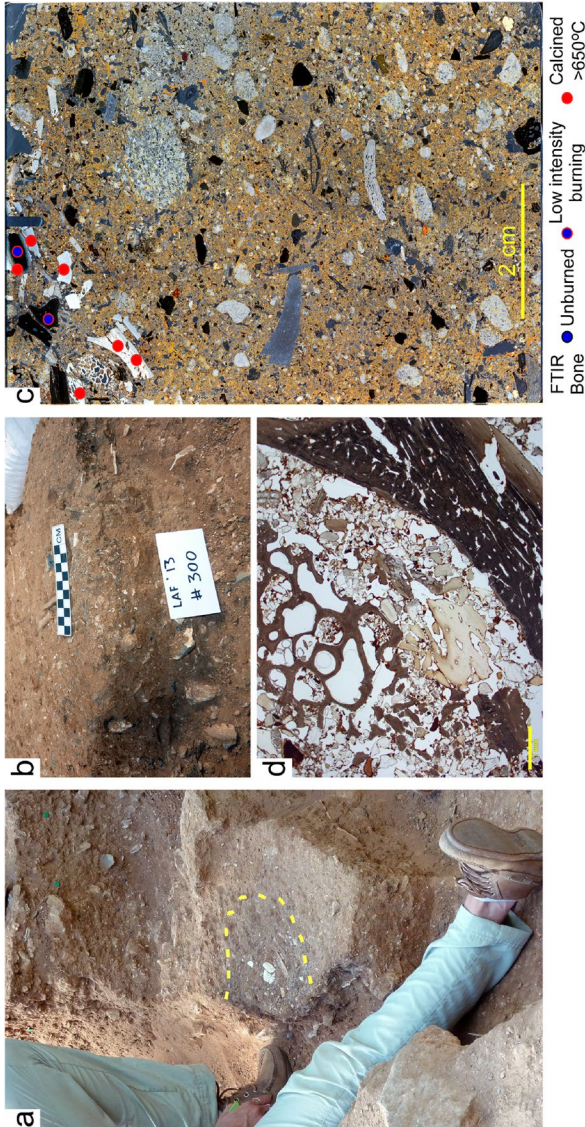
As a whole, Layer 1 locally exhibits beds, lenses, and stringers of cm-sized limestone clasts, which become coarser (~10 cm in diameter) and blockier toward the bedrock walls and floor to the north. There, vertically standing platy clasts are detached from the wall and floor. The top of Layer 1 is undulating, irregular, and incorporates some of the overlying yellower sediment of Layer 2.

*Micromorphological observations:* The lowermost part of the unit has coarser materials, especially coarse quartz sand, chert, iron-rich grains, limestone (often etched), all of which are crudely bedded. The fine fraction occurs as braces (gefuric c/f related distributions), iron-rich clay coatings (chitonic c/f related distributions), and cappings composed of iron-rich silty clay. The upper part of the unit exhibits incipient weakly bedded, banded fabric and silty cappings on larger components (Fig. 8).

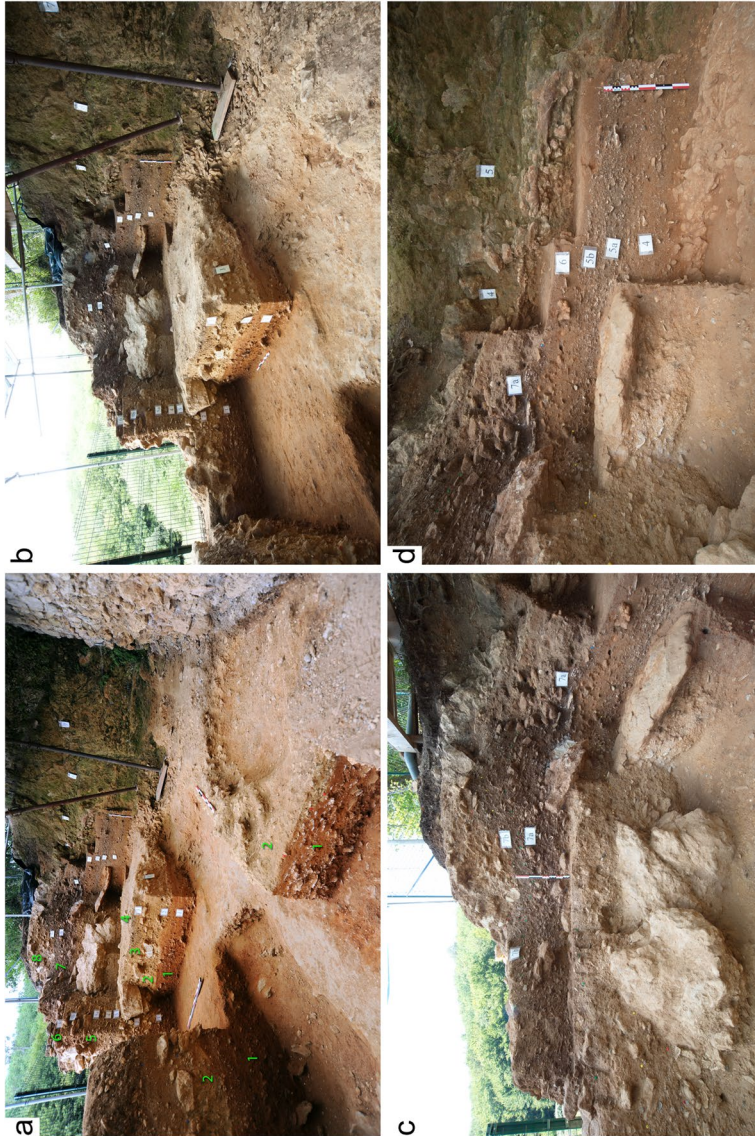
**Layer 2. Field observations:** Consists predominantly of yellow (10YR7/6; some areas are strong brown, 7.5YR5/6) partly cemented, calcareous sand, rich in limestone clasts, which vary laterally from dm to cm in size (Fig. 9). In the west profile, the layer incorporates larger dm-sized limestone blocks of roof fall. Layer 2 is thickest in its W and NW parts (~25 cm) and thins to the SE (~12 cm); in plan-view, the orientation of the deposits is NW–SE. Along the northern wall, limestone clasts vary from blocky to platy and are consistent with cryoclastic detachment from the wall. The lower contact with Layer 1 is wavy, erosional, generally sharp, and is oriented to the SE, matching the overall orientation of the deposits.

*Micromorphological observations:* Overall, in thin section the deposits from Layer 2 are dominated by rounded, sand-sized limestone clasts that are often slightly sorted and intermixed with common bone fragments, which display different degrees of thermal alteration and are often rounded. The calcareous deposits show frequent well-developed banded fabrics and calcareous silty and sandy cappings on mm-sized and larger clasts. The cappings are red, iron rich, and silty; they are more subdued in transmitted light but somewhat more striking in oblique incident light (OIL) and darkfield illumination.

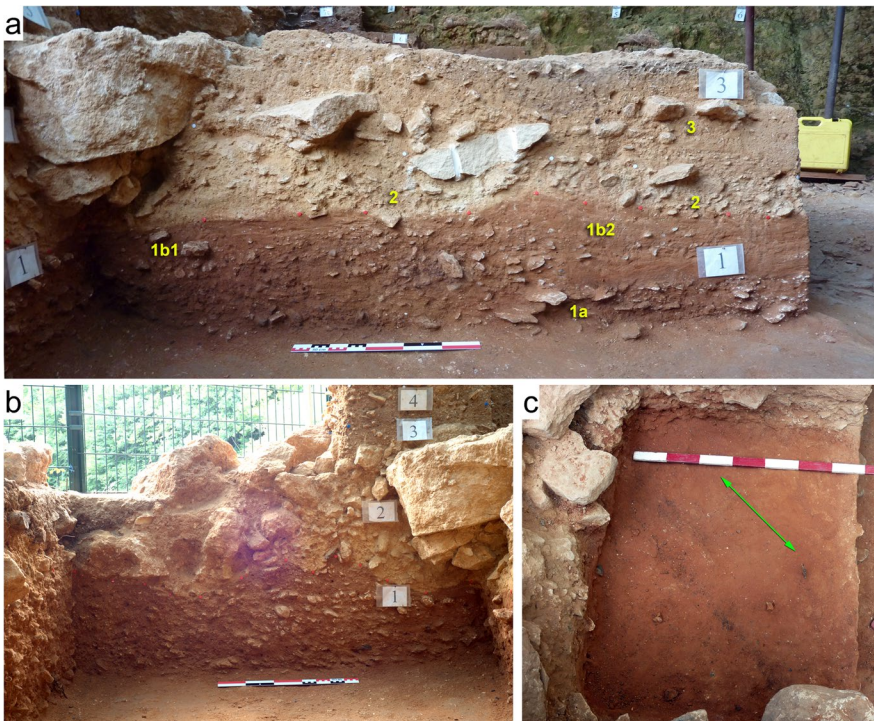
**Layer 3. Field observations:** Consists of strong brown to reddish yellow (7.5YR5/6 to 6/6) poorly sorted, silty, coarse to medium sand. The layer is



**Fig. 5** Possible fire feature in Layer 4, square I4. (a) Large view of the feature whose limits are marked by the dashed yellow line. (b) Close-up showing the narrow width (~10 cm) and depth (~4–5 cm) of the feature, with the general location of micromorphological sample LAF300. (c) Dark field thin section scan of sample LAF300, showing a concentration of small burned, including calcined, fragments in the upper 2–3 cm. The circles note microFTIR measurements on bones and their degree of burning. (d) Photomicrograph showing abundant bone fragments, some calcined and with in situ fragmentation, PPL, scale is 1 mm



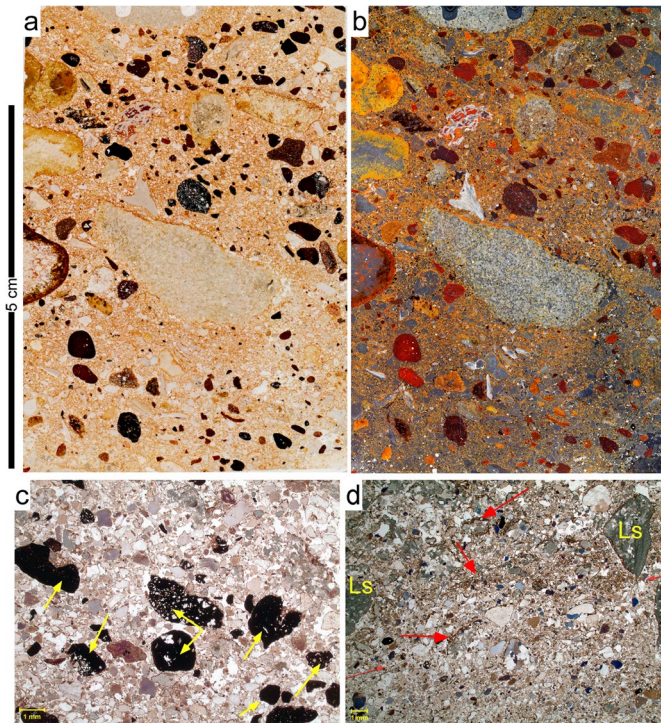
**Fig. 6** Views of the stratigraphic profiles in the Western Sector. Scales are 50 cm. (a) looking northwest from the southeast corner of the excavation; numbers in green correspond to the identified layers; (b) view looking roughly West. Beyond the deposits is the site fence and the Departmental road; (c) close-up view of the upper Mousterian deposits (Layers 4, 5 and 6) and the darker Upper Paleolithic deposits (darker Layers 7) which has been eroded and filled with the yellow channel deposits of Layer 8 above; (d) View looking north showing layers 4 through 7a, the latter partially excavated



**Fig. 7** Field view of basal layers 1, 2, and 3 in the Western Sector; (a) Northern face of excavations in squares I4–I5, with stratigraphic units labeled in yellow. Note the textural variations and unit subdivisions within Layer 1, the sharp erosional contact between Layers 1 and 2, and the increase in roof collapse from Layers 2 to 3, marking the initial phases of the collapse of the roof; (b) Western face of excavations in square I4 showing Layers 1 through 4. Note the sharp, undulating contact between Layers 1 and 2 and the abundance of unbedded and rounded limestone blocks that are also included in Layer 3; (c) Plan-view photograph of the small channels with iron-rich clasts in Layer 1 with the arrow paralleling the NW–SE orientation of the channels; scales with 10 cm increments

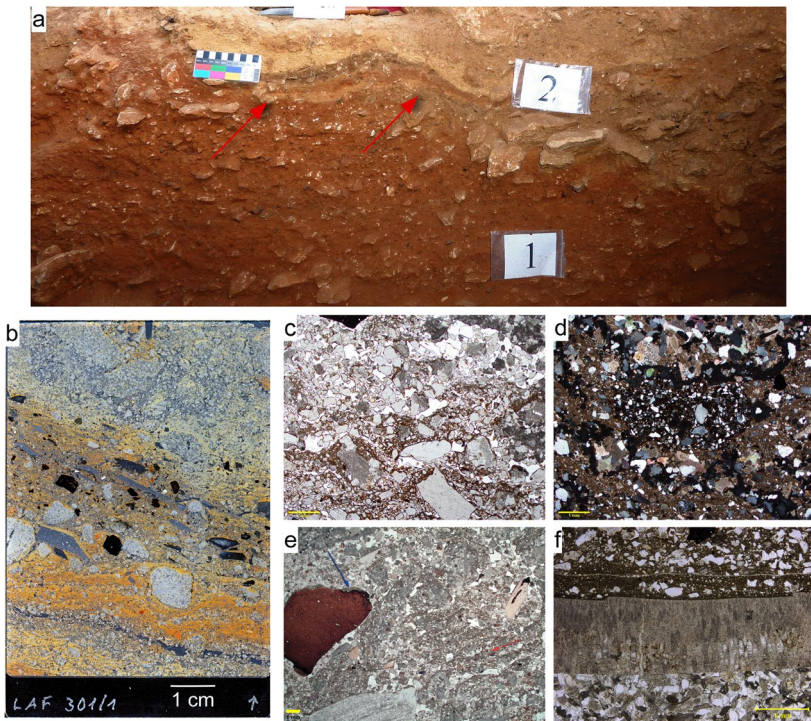
generally flat lying, with little or no apparent dip or inclination, and it essentially fills in the undulating, irregular SE sloping relief of the surface of the underlying Layer 2. The erosional Layer 2/3 contact is inclined towards the south and drops ~25 cm over 6 m. In the western part of the excavation (sq. I3), large limestone blocks correspond to episodes of roof fall that began in Layer 2 times but became more prominent during the accumulation of Layer 3. It also contains local concentrations of rounded cm- and pea-sized limestone gravel and a number of diffuse concentrations (10 to 15 cm in diameter) of cm-sized burned bone fragments that appear to represent poorly defined or preserved combustion features; microstratigraphic organization of components typical of in situ combustion are lacking.

Layer 3 is at least 40 cm thick but thins to the north (towards the cave wall) where it is about 10 cm thick.



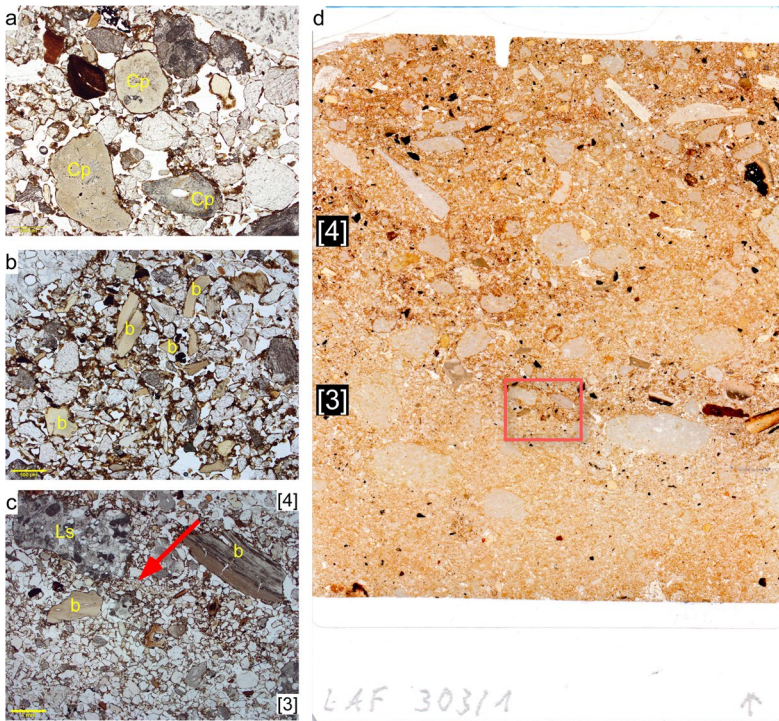
**Fig. 8** Micromorphology of Layer 1 with thin section scans in plane-polarized light (PPL) (a) and in dark-field (b) of sample 104B. Note the coarse bedding of the components, particularly visible in the iron-rich grains, and some cappings on the large limestone grain in the center; (c) Photomicrograph of bedded iron-rich clasts (yellow arrows) in Layer 1, (sample 10–2; sq. F6), PPL, scale is 1 mm; (d) PPL view of Layer 1 (sample 10–3; sq. F5) uppermost deposits, here with crudely bedded quartz and calcitic sands and silts, alongside larger sub-rounded limestone fragments (Ls). In this view, domains of crudely developed cappings are clearly visible (red arrows), scale in 1 mm

*Micromorphological observations:* Under the microscope, the deposits of Layer 3 are poorly sorted, with very frequent calcitic grains (silt- to granule-sized), quartz sand, common coprolites, and bones (Fig. 10). The last are present as cm-sized, commonly burned fragments, and as smaller, medium to coarse sand-sized, rounded clasts. The almost uniform scatter of rounded clasts throughout the deposits and locally granular domains suggests bioturbation. The calcite-rich sandy fine fraction originates from mechanical breakdown of the limestone; these grains show signs of dissolution and etching towards the uppermost parts of Layer 3. Poorly sorted dusty clay coatings are widespread. In samples near the cave wall, several phases of calcium carbonate cementation are discernable, starting with carbonate-impregnated yellow matrix, which is then decalcified; in turn, it is followed by the formation of clay coatings and, finally, the presence of sand-sized circular calcitic hypocappings associated with modern rhizoliths. The contact with Layer 4 above is sharp and clear and, locally, a 250  $\mu\text{m}$ -thick phosphatic crust is present at this contact.



**Fig. 9** Field and micromorphological views of Layer 2; (a) Eastern profile in squares F7 with red arrows indicating Layer 2 solifluction deposits (scale is 10 cm); (b) Dark field thin section scan of Layer 2 (sample 301; sq. F7) with well-developed silt and clay cappings on top of larger mm-sized limestone clasts overlying darker brown layer with common (10–25%) burned bones (black in this view), scale is 1 mm; (c) Photomicrograph of thin Sect. 301/1 showing well-developed silty cappings, in PPL, scale is 1 mm; (d) Same as (c) but in XPL, note the calcitic nature of the matrix; (e) Photomicrograph with well-developed banded fabric (red arrow) in sample FER-10-1 (sq. G6), and bone fragments, some showing calcareous silty cappings (blue arrow), in PPL scale is 1 mm; (f) Detail of thick calcareous sandy and silty capping on oyster bioclast derived from the limestone (sample 110; square G6), in PPL, scale is 1 mm

**Layer 4. Field observations:** Layer 4 is exposed mainly in squares I4 and K5, where it is ~17 cm thick. Only thin remnants are visible elsewhere, as the upper part was removed by Peyrony during previous excavations. It is massive, compact, reddish yellow (7.5 YR 6/6), silty medium sand with relatively abundant cm-sized pieces of bone (many are highly fragmented and burned) and chert. A feature (~10 cm wide and ~4–5 cm deep) exhibits a concentration of mm-sized burned bone fragments (some calcined) and resembles a poorly preserved remnant of a small (~cms across) combustion area in square I4 that consists of darker sediment with abundant burned bone. Near the northern cave wall, Layer 4 is a 10–20 cm-thick veneer of yellowish red (5YR 4/6) sandy sediment (relatively rich in quartz) abutting the vertical, irregular cave wall. This sandy lithology relates to its proximity to the north wall where decalcification and decomposition of the bedrock has resulted in liberation



**Fig. 10** Layer 3; (a) Common (10–25%) rounded coprolite (Cp) grains with fine iron-stained clay coatings around the clasts and common intergrain porosity (sample 211; square G7), in PPL, scale is 500  $\mu\text{m}$ ; (b) sand-sized bone fragments (b) dispersed in the deposits (sample 211; square G7), PPL, scale is 500  $\mu\text{m}$ ; (c) Contact between Layers 3 and 4 (numbers in brackets) (sample 303.1; square J4) displaying bone fragments (b) and limestone clasts (Ls). Note the clear, sharp contact between the loosely packed granular deposits of Layer 3 and the more compact matrix-rich deposits of Layer 4 above it, in PPL, scale is 1 mm; (d) thin section scan of sample 303/1 showing the contact between Layer 3 below and Layer 4 above. Note the relative abundance of anthropogenic materials in Layer 4 when compared with Layer 3 deposits. The red square marks the location of photomicrograph shown in (c). Thin section is 6 cm wide

and enrichment of quartz sand, which is coated and stained with red, iron-rich clay. Similarly, rounded and corroded limestone pebbles were noted in this area.

The lower part of the layer is mostly sub-horizontal, but its inclination — generally toward the SE — clearly increases in its upper part, albeit slightly. Layer 4 continues out to square I2 near the road, where it is sandwiched between large blocks of roof fall (that fell during Layer 3 times) and locally massive roof collapse in the overlying Layer 5. In most excavated areas, Layer 4 grades smoothly into the overlying Layer 5.

*Micromorphological observations:* The fine fraction is composed of loosely packed grains of quartz and limestone sand with red limpid clay matrix as coatings and bridges (chitonic and gefuric *c/f* related distributions, respectively) — Fig. 11. The coarse fraction includes abundant cm-sized bones that are commonly burned and locally bedded; some larger, angular to subangular bones might have been



trampled, as shown by several instances of in situ fragmentation. Also abundant are cm-sized angular chert flakes and smaller, mm-sized fragments of fat-derived char. Other coarse fraction elements include sand-sized pieces of coprolites and few earthworm biospheroids. Remnants of combustion features are suspected and are comprised of horizontally lying burned bones and char, although no ash and rarely altered substrates were found; associated pieces of limestone do not appear to have been burned. The feature in square I4 is ~4 cm thick and shows a concentration of small bone fragments, some calcined and with in situ fragmentation; the sediment below is slightly, but clearly rubified. There is no ash, but some charcoal is present.

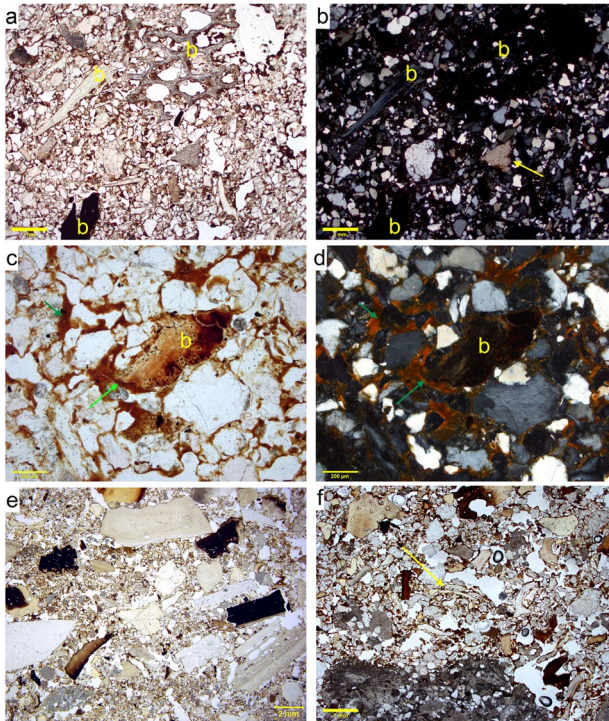
As noted in the field, a large degree of variability exists among samples collected close to and away from the cave wall in the north. Close to the cave wall, the deposits are decalcified, proportionally enriched in quartz sand, and show abundant etching of limestone clasts; the coarse fraction is bedded because of water flowing next to the cave wall. Away from it, the fine fraction with calcitic granules and silt is still present, with decalcification only in restricted domains. Likewise, limpid red clay coatings vary according to distance from the wall: they are thicker and more pervasive in samples near the cave wall. Calcitic hypocoatings associated with modern rhizoliths are superposed on the clay coatings and are partially decalcified.

**Layer 5. Field observations:** Layer 5 varies in thickness from about 50 cm in the west profile to ~30 cm along the north wall. Layer 5 was subdivided into two units, 5a and 5b, which are overall similar but differ in the amount of fine fraction and density/size of anthropogenic inputs, the latter being higher in Layer 5a.

In the west profile (sq. I4), *Layer 5a* is 15 cm thick and is composed of reddish yellow (7.5YR6/6) pebbly silty sand with generally platy limestone clasts and bone fragments. To the NW (sq. J3), it abuts against dm-sized roof fall and, in that area, Layer 5a grades into the overlying Layer 5b. In the westernmost part, Layer 5a is inclined (~4° apparent dip) and contains ~20 cm-sized limestone clasts; it abuts against large, dm-sized blocks of roof fall exposed in a profile facing the road.

*Layer 5b* is 30 cm thick in the west profile and only ~13 cm thick along the north wall. In square I4, Layer 5b also has a more granular appearance, is richer in rounded limestone pebbles (~0.5 to 1 cm in diameter) and contains relatively fewer bones than in 5a. Along the north wall there are no limestone components. Overall, the apparent dips follow what was described for Layer 5a, both in the west and north profiles: in the north profile the apparent dip is to the east, whereas in square I4 it appears to dip to the SSE. The contact with the overlying Layer 6 is clear, sharp, and has an inclination similar to those of the apparent dips of Layer 5.

**Micromorphological observations:** The deposits of Layer 5 are overall like those previously described for Layer 4, with frequent lithic materials, char, and bones, which are commonly burned (Fig. 12). Other coarse fraction components are common limestone clasts and few coprolites. The lateral variation matches that of Layer 4, with increased decalcification near the wall (seen by common etching of the few limestone fragments still present) and more calcareous components away from it. There are two types of clay features. The first is localized, very thick, poorly sorted, reddish-brown clay infillings, which have very fine inclusions (speckled). The second type of clay consists of void coatings of uniform thickness comprised of fine



**Fig. 11** Layer 4; (a) Photomicrograph of sample 5A (square L5) collected near the cave wall showing angular bone fragments and splinters (b) in a sandy, quartz-rich matrix, PPL, scale is 1 mm; (b) same as (a) but in XPL, revealing quartz-rich matrix and etched limestone grain (yellow arrow); (c) Weathered bone fragment (b) and localized red, limpid, laminated clay coatings (green arrows—sample 5A; square L5), scale is 200  $\mu$ m; (d) same as (c) but in XPL. Note the angularity of many of the quartz grains, signaling their derivation from the limestone; (e) Photomicrograph of sample 207a, square I5, further away from the cave wall; note the burned bones, some of which are calcined, in PPL, scale is 2 mm; (f) Photomicrograph of sample 207a, primarily loose, sand-sized fragments of burnt bones and limestone. Note the trampled fish bone in the center (yellow arrow), in PPL, scale is 1 mm

dusty clay. Both types of clay features formed after the decalcification of the deposits and are, in turn, postdated by the formation of common calcareous hypocoatings.

Away from the wall, in square K3, the deposits overlie and infill the relief caused by the fall of dm-sized limestone clasts from the roof, resulting in localized bedding of the coarse components. This is particularly true for the somewhat platy limestone clasts that are roughly 1–2 cm across. Here, and towards the south, the deposits are matrix supported with a fine fraction composed of calcareous silty clay in a close porphyric-related distribution. In the area of square I4, the calcite appears to be fresher in Layer 5 compared to that in Layers 4 and 3 in this same area.

**Layer 6.** *Field observations:* Layer 6 has a distinct, sharp boundary with Layer 5 and is a uniformly compact massive strong brown (7.5YR 5/6) silty fine sand with some mica and some angular limestone fragments at the top; there are also scatters of chert and bone, some of which are calcined. Layer 6 is well defined along the

north wall but more difficult to delineate along the NW and west profiles where it is much more calcareous and not as well sorted. It appears to be archaeologically richer in these latter areas in comparison to its occurrence along the north wall; it also has rounded limestone pebbles (as in Layer 5), and a few clasts of bedrock, 10 to 15 cm in size. Layer 6 is 15 to 20 cm thick in the west profile (square I4), whereas along the north wall it is more lithologically homogenous, with well-sorted fine sand and decalcifying limestone clasts. The dips are the same as those in Layer 5, with an overall inclination to the SE. In the west profile, Layer 6 overlaps the large limestone block that fell during Layer 5 times. Layer 6 has a clear, sharp contact with Layer 7 above.

*Micromorphological observations:* Near the wall, the layer consists of decalcified quartz sand, with common iron-stained, rounded granular and sand-sized bones, some burned. Iron-rich dusty reddish-brown clay coatings occur along with braces and partial infillings. Prevalent calcareous hypocoatings, which postdate the clay coatings, are now being dissolved (Fig. 13).

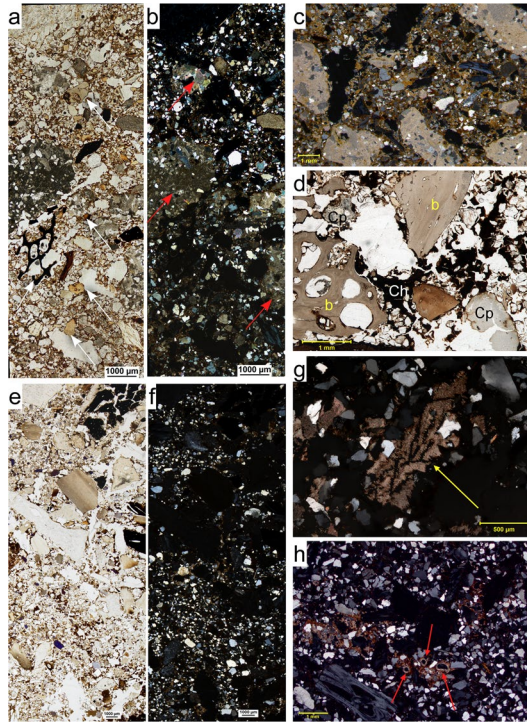
Away from the wall, the matrix is dusty silty-clay with calcareous silt and sand, and more anthropogenic inputs, including fine, mm-sized burned bones, rare char, and few chert flakes. Pebble and sand-sized limestone clasts are common and vary from rounded to more angular; some are rather platy. Limpid red clay coatings are common and locally well developed.

*Layer 7. Field observations:* Layer 7 can be traced across from the west profile to the north profile. Overall, it consists of compact, brown (7.5 YR 4/4) sandy silt with abundant lithics and bone (Fig. 14). Its maximum thickness is about 55 cm (square K3), although the upper part of this layer was previously excavated and some of it is missing. Nevertheless, in the NW corner of the excavation (square L3), the upper part has been truncated by the gravelly channel deposit of Layer 8 (see below), and it is capped by dm- to m-sized blocks of roof fall. Possible earthworm burrows were noted. Layer 7 was subdivided into three parts: 7a, 7b, and 7c.

- **7a** is massive reddish brown to brown (5YR 4/4 to 7.5YR 4/4) bedded silty sand containing abundant bones (many burnt), lithics, and generally rounded dm-sized limestone blocks.
- **7b** differs from Layer 7a in being finer grained, and having fewer limestone clasts, a greater proportion of sand, and smaller anthropogenic component.
- **7c** is a small lens at the top of 7B in square K3 and is truncated by Layer 8 both in its upper part and towards the south. It is about 10 cm wide by about 10 cm thick and consists of sandy silt.

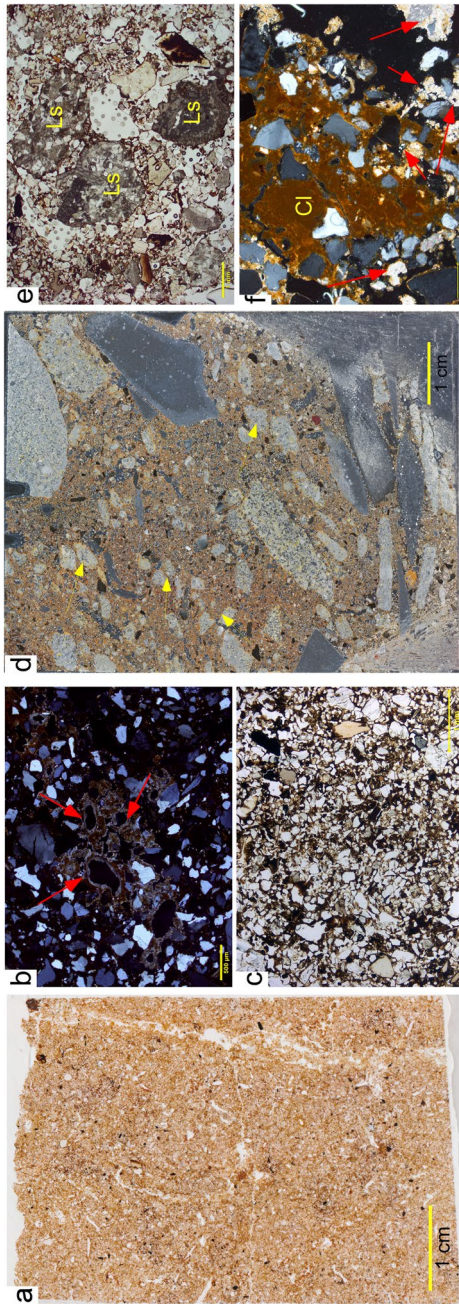
The cone morphology of the deposits is represented in the west profile by dips to the south where they mainly follow the slope of the large blocks of roof collapse visible from the road. As mentioned for Layer 5, the source of this material points to the apex of a cone that was situated above the present-day road. Along the north wall, the deposits are inclined to the ESE, and in the west profile (square J3) along the medial axis of the cone, the dip direction changes to the SSE, following radially across the cone.

*Micromorphological observations:* Overall, Layer 7 exhibits similar decalcification near the wall as in other layers and is increasingly calcitic away from the wall

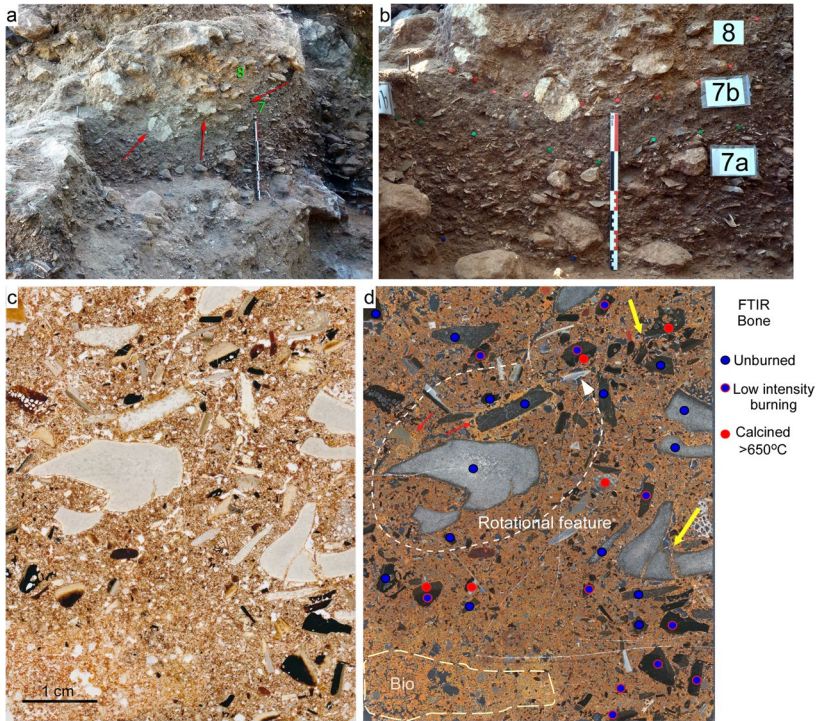


**Fig. 12** Layer 5 away and close to the cave wall; **(a)** Composite photomicrograph of sample 201 (square I4) — away from cave wall — showing frequent bones, including sub-rounded fragments (white arrows) mixed with cm-sized bone fragments with different degrees of burning, in PPL, scale is 1 mm; **(b)** same as **(a)** but in XPL; Note the presence of limestone clasts (red arrows) in this area; **(c)** Microphotograph of sample 200b (square I4) with sub-rounded and rounded granules of limestone in a silty sandy matrix that incorporates common bones spinters, in XPL, scale is 1 mm; **(d)** photomicrograph showing burned bones fragments **(b)**, char (Ch) and coprolites (Cp) that are frequent throughout Layers 5a and 5b, in PPL, scale is 1 mm; **(e)** Composite photomicrograph of sample 106a (square L5) — near the cave wall — with abundant bone fragments, in PPL, scale is 1 mm; **(f)** same as **(e)** but in XPL. Note the lack of calcareous material because of decalcification in this area of the site; **(g)** limestone clast in sample 106a showing etched edges (yellow arrow) denoting strong decalcification; Note also the presence of silt-sized sub-angular quartz grains from the limestone that get released into the sediments with the loss of the calcareous cement, in XPL, scale is 500  $\mu$ m; **(h)** calcitic hypocoating associated with rhizoliths (red arrows) in sample 106a, in XPL, scale is 1 mm

to the south (Fig. 15). The matrix is very dusty overall, and near the wall it exhibits calcitic silt and common dusty fine material, which differentiates it from the layers below. Moreover, rounded cm-sized limestone pebbles occur as described in the underlying layers. One important aspect is the relatively high frequency of iron staining of the bones in Layer 7, which occurred prior to their deposition in this area, since neither the matrix nor the limestone is stained. In thin section, there is no apparent bedding of the quartz or limestone materials. Rare rotational features were identified.



**Fig. 13** Layer 6; (a) thin section scan of sample 109 (square L5) near the cave wall; note the compact, sandy, well-sorted nature of the deposit that here reflects decalcification along the cave wall, scale is 1 cm; (b) Photomicrograph of sample 109 with quartz-rich sand with few anthropogenic inputs and absence of limestone grains due to decalcification. Note, however, the calcitic hypocoatings (red arrows) representing the presence of more recent rhizoliths, in XPL, scale is 50  $\mu\text{m}$ ; (c) sample 109 showing the presence of sand-sized bones in the quartz-rich deposits, in PPL, scale is 1 mm; (d) scan of calcite-rich Layer 6 in sample 114b (square L4) showing two populations of limestone clasts, cm-sized rounded ones (yellow arrows) and larger more platy clasts, scan in dark-field, scale is 1 cm; (e) sample 114b showing the characteristic calcareous nature, including rounded granules and sand-size limestone clasts. Note the angular fragments of bones (b) with different degrees of thermal alteration, in PPL, scale is 1 mm; (f) sample 114, closer to the cave wall and showing clay-rich domains (Cl), sand-sized quartz and limestone grains (red arrows), in XPL, scale is 200  $\mu\text{m}$



**Fig. 14** Field and thin section views of Layers 7 and 8; **(a)** Layer 7 being cut by a channel of Layer 8 with a sharp contact (red arrows). **(b)** Detail of contact between Layers 8 and 7 as shown by red pins in the photograph. **(c)** Thin section of sample 111 (square L4) from Layer 7 showing angular limestone clasts, along with abundant cm-sized angular bones exhibiting different degrees of thermal alteration within a compact matrix of reddish brown dusty silty clay. Note the overall fine-grained and dusty appearance of the sediment. PPL, scale is 1 cm; **(d)** dark field scan exhibiting some trampling as shown by in-place fractured bones (yellow arrows), along with some burrowing in the lower left (Bio). Red arrows indicate localized calcitic hypocrotings. Note the rotational feature, which indicates downslope movement of material, possibly related to its position proximal to the apex of the depositional cone. The circles note microFTIR measurements on bones and their degree of burning

**Layer 8. Field observations:** Layer 8 is a gravelly channel deposit that truncates much of Layer 7. It is best exposed in the northwest corner of the excavation (square J3). It is a poorly sorted mixture of mm-sized rounded pebbles and cm-sized platy clasts of limestone; the larger limestone clasts have rounded edges from dissolution, although some are very angular. There is virtually no fine matrix, and anthropogenic components are rare. In the field, there is no apparent bedding of the clasts, although in thin section, some bedding is visible. The direction of flow within the channel cannot be accurately determined because it is visible only in one profile; a similar type of deposit appears along the north wall where it occurs between a large piece of roof fall and the bedrock. Both occurrences point to localized channel erosion and dissection of the cone emanating from the area of the Upper Cave above.

*Micromorphological observations:* The micromorphology of Layer 8 is best typified in sample 206 (square K3). It is composed of rounded to well-rounded fresh limestone grains that range from predominantly sand- to cm-size, although smaller sizes are rarer (Fig. 16). It is generally clast supported except for localized domains that are slightly richer in finer, silt- and sand-sized material that form bridges and interstitial spaces between the coarser limestone grains (these are possibly passage features). Some bones are present, and sand-sized ones are rounded; larger, cm-sized bones tend to be angular. It is weakly bedded at the base and center of the slide and much less so at the top. Clay coatings are of two types: (a) void coatings composed of clear, finely laminated clay that coat only some of the coarse components; and (b) discontinuous dusty red brown clay coatings. Calcitic hypocoatings are associated with locally abundant rhizoliths.

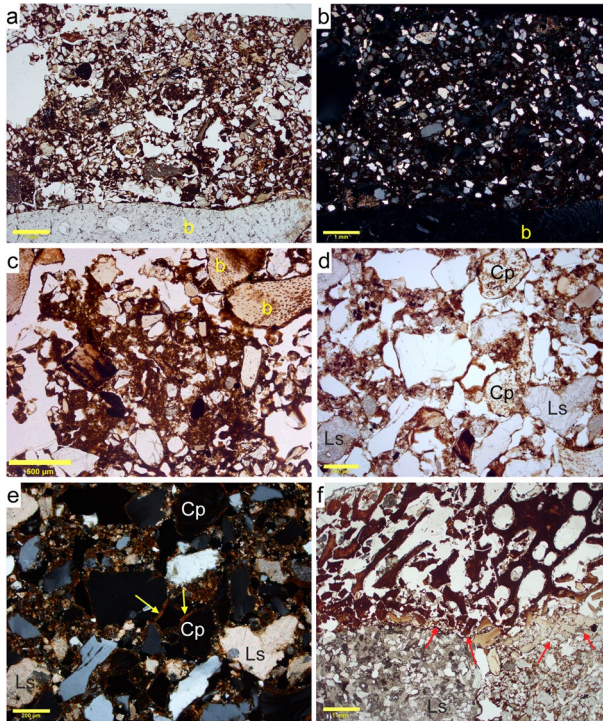
**Layer 9.** *Field observations:* Layer 9 is a cm-thick spatially restricted sandy deposit that occurs in patches on a bedrock sill that separates the western/northern portions from the Upper Cave (square M4). It is composed of partly cemented, mottled light brown silty quartz sand with many (potentially recent) calcitic root hypocoatings that locally impregnate the matrix. It is extensively bioturbated with many cm-diameter insect burrows.

*Micromorphological observations:* The one sample (square M4) from this layer shows cultural debris as an unsorted jumble of large flints and bones, several of them burned. The crude bedding is inclined toward the main excavation. Overall, the deposits are cemented by calcite, with numerous rhizoliths; a final stage of burrowing occurs with loose quartz grains that exhibit iron clay coatings.

## The Stratigraphic Sequence in the Northern Sector

We identified five main layers in the deposits excavated in the Northern Sector (Fig. 17) and present here more in-depth data on their sedimentological and microscopic descriptions. The descriptions are based on lithological criteria. In any case, note that the sediments differ markedly from those in the Western Sector in being richer in fine material, especially reddish clay in the upper part.

**Layer A (Archaeological Layer (AL) LAF8-5).** *Field observations:* This is the lowermost layer exposed in the field and is ~10–15 cm thick. It is a yellowish red (5YR 4/6) clayey-silty sand, with granules and rounded pebbles of limestone < 1 cm in diameter. Towards the base, larger *plaquettes* of angular limestone appear and some are inclined vertically, running sub-parallel to the wall behind the excavated profile. Surrounding some of the limestone grains is an amber brown weathering crust. Two stony features were revealed during the excavation (Fig. 18 and see Figure 26 below). The first is an entire ‘mound’ that consists of an elongated raised mass composed of laterally variable tilted pieces of limestone clasts; several of these are well rounded and in profile are domed upward. The feature was not completely exposed, but its lateral dimensions are at least ~30 cm across, ~10–15 cm high, and at least 30 cm long. The upper contact with Layer B is distinct and it seems to be slightly inclined towards the NW. The second feature is similar and occurs ~1 m to the NE of the first.

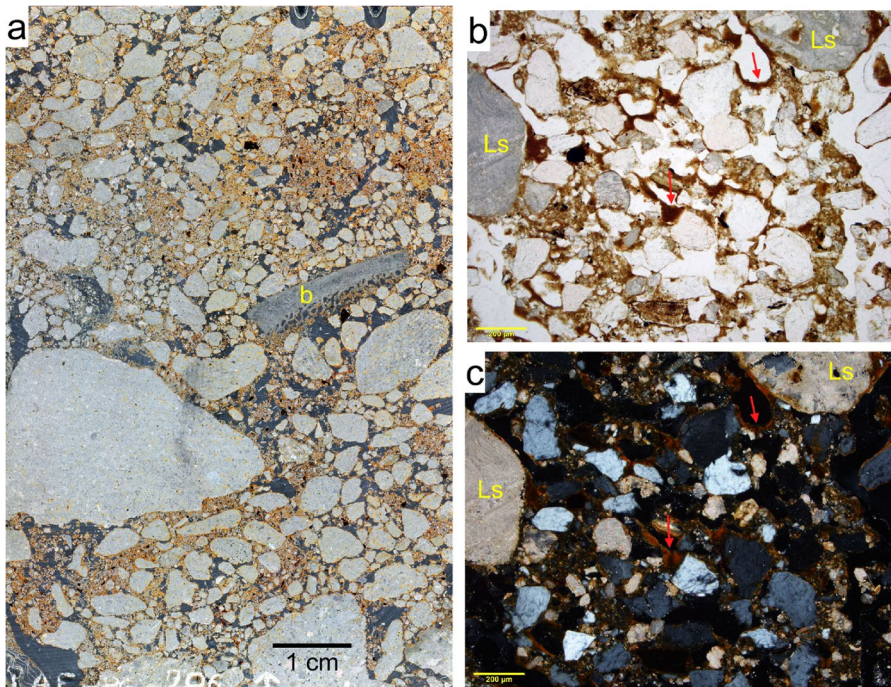


**Fig. 15** Photomicrographs of Layer 7; (a) sample 111 (square L4) is close to the wall and shows bone (b) at base overlain by dusty silty clay aggregates with common sand-sized bone splinters, and coprolite and quartz grains, PPL, scale is 1 mm; (b) same as (a) but in XPL. Note the predominance of siliceous, non-calcareous materials; (c) detail of aggregate showing the dusty fine silty clay matrix, along with inclusions of quartz sand and silt. Note the iron staining of the bone, PPL, scale is 500  $\mu$ m; (d) sample 310 is away from the wall (square J3) and shows dusty, silty clay between the granular elements of sand-sized quartz, coprolites (Cp), and calcite grains from the limestone (Ls); PPL, scale is 500  $\mu$ m; (e) same as in (d) but in XPL; note the reddish brown clay coatings (yellow arrows); (f) sample 302 (also in square J3) shows an example of crushed burnt spongy bone (red arrows) overlying a fragment of limestone (Ls), PPL, scale is 1 mm

*Micromorphological Observations:* Micromorphologically, the mounds at the base of the profile in **Layer A** consist of laterally variable tilted limestone pieces, several of which are well rounded (Fig. 19). Well-developed laminated silt cappings occur with coarser and finer layers and some with laminated red clay stringers within the silt cappings; there is a weak platy microstructure in domains that are richer in matrix, and, in certain localized areas, this structure grades into a poorly developed banded fabric (Fig. 18c). Some bones occur. Very fine iron-rich red coatings represent the final post-depositional stage.

**Layer B (AL LAF8-4).** *Field observations:* This unit, which is about 35 cm thick, consists of reddish yellow (7.5YR 6/8), massive, compact, silty quartz sand with yellow brown silty clay aggregates and coatings. Some washed zones among the quartz sand grains are visible in hand lens. It contains platy and blocky (equant), cm-sized



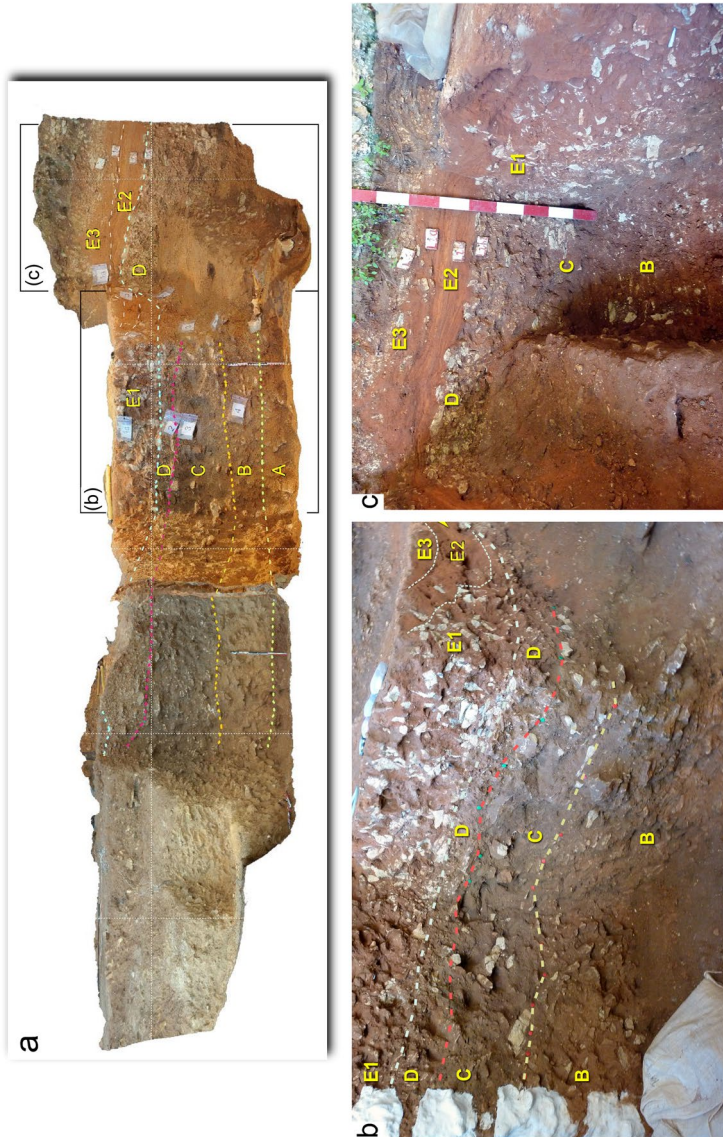


**Fig. 16** Thin section of Layer 8, sample 206 (square K3); (a) dark field thin section scan showing a striking number of well-rounded, circular to sub-circular, mm- to cm-sized clasts of fresh limestone; these are bedded at the base and less so at the top. It is generally clast-supported, but with some domains rich in silt- and sand-sized grains; note the platy bone fragment in the middle (b), scale is 1 cm; (b) photomicrograph in PPL showing generally clast-supported quartz and limestone (Ls) sand with aggregates and domains of dusty calcareous sand and silt; also note layered, slightly dusty, reddish brown clay coatings (red arrows), scale is 200 µm; (c) same as (b) but in XPL showing more distinctly the clay coatings; scale is 200 µm

limestone clasts, which are locally concentrated, weakly bedded and inclined to the NW. Some weathered limestone granules and pebbles exhibit thin coatings of yellow brown clay that are much thinner than those in overlying layers E1 and D.

*Micromorphological observations:* red iron clay coatings are not present in Layer B, and burnt bones begin to increase in comparison with the underlying deposits. Layer B has clear, well-developed banded fabric and typically, rounded grains of phosphatized limestone.

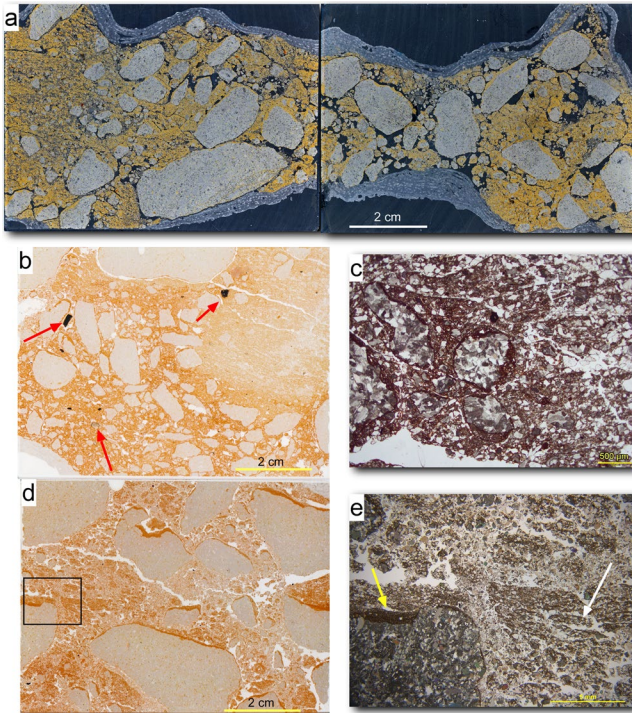
**Layer C (ALLAF8-3).** *Field observations:* This layer (~20–25 cm thick) consists of soft, brown to dark brown (7.5YR 4/4 to 7.5YR 3/4) sand, which, viewed with a hand lens, is comprised of washed quartz sand and darker domains or aggregates of brown silty clay. Some 10 cm-sized burrows are visible, and much of the layer could be burrowed. It appears to dip slightly to the NW and contains platy, cm-sized limestone clasts that are more numerous and more strongly inclined to the west than below. In addition, some brown clay coatings occur in voids and some around grains



**Fig. 17** View of stratigraphy in Northern Sector, (a) an orthorectified photo of the profiles where the labelled rectangles depict the location of the photographs shown in (b) and (c); Note that the color differences in (a) is due to natural sunlight versus hallogen lamps. (b) View of profiles looking towards NW before excavation in 2014, shown with stratigraphic units. (c) View of north profile against bedrock with main stratigraphic units; red tags indicate Delporte's stratigraphy. Note that photos in (b) and (c) are not rectified and the apparent dips in these photos do not reflect the actual layer inclinations



**Fig. 18** Field view of stony features excavated in Layer A; (a) view facing northwards of 'mound' that consists of an elongated raised mass with limestone clasts (arrow); (b) view facing westwards of vertically inclined angular limestone clasts



**Fig. 19** Thin sections from the lower part of the LAF8 sequence. (a) Dark field scans of stony feature in thin sections (sample 413), Layer A. Note the upturned nature of the rounded limestone class, showing generally well rounded, slightly platy limestone clasts with cappings of red silty clay and granular aggregates of red silty clay; The upturned nature of the limestone clasts is a result of freeze–thaw, scale is 2 cm; (b) Thin section scan of sample 414 from contact between Layers A and B showing a lateral contact between yellow calcareous sand and silt with banded fabric and red clay-rich matrix with coarse limestone grains that are rounded and have thick silt coatings. Few bones (possibly burned) are present (red arrows), scale is 2 cm; (c) Photomicrograph of sample 414 showing cryoturbated grains and banded fabric associated with cold climatic conditions affecting the deposits, PPL, scale is 500 μm; (d) Thin section scan of sample 408 from Layer B showing well developed banded fabric with link cappings and abundant cappings on limestone clasts. The cappings tend to be laminated, with red dusty clay, followed by fine silt with few sand grains and a final state of coarser silts and sands, PPL, scale is 2 cm; (e) Photomicrograph of area marked by black square in (d) where features associated with cold conditions such as silt cappings (yellow arrow) and domains of banded fabric (white arrow) are visible, PPL, scale is 5 mm

of rounded limestone. This unit pinches out to the north on the east profile. The contact with the overlying Layer D is sharp (Fig. 20a).

*Micromorphological observations:* Layer C is a remarkable layer with a complex depositional history. It is comprised of several phosphatized grains (Fig. 19e) that include limestone and complex aggregates of matrix-like material with incorporated bones. These deposits seem to have been bioturbated in antiquity. They were subsequently affected by cold, with silt cappings developed on all the coarse materials: both on the fresh limestone fragments, on the phosphatic aggregates, and on the cultural materials (bones and flint). There are domains

**Fig. 20** Micromorphological aspects of the upper part of the Northern Sector sequence, Layers C, D, E1: (a) composite thin sections of sample 406 showing the contact with Layer E1 and Layer D (dashed yellow line) and Layer C in the two lowermost scans. Note the presence of numerous, often sand-sized, burned bone fragments within a generally fine reddish-brown silty clay matrix. The insets to the left show detail aspects related to frost-action throughout the deposits, namely frequent laminated cappings on coarser components, domains with granular microstructure, domains with weakly developed lenticular microstructure and coarser domains with washout finer matrix. Scale of all scans is 1 cm; (b) photomicrograph in Layer E1 showing cappings on limestone and iron-rich clasts and a subsequent stage of thick laminated clay coatings (arrow). Not visible here is the partial decalcification of the matrix, PPL, scale is 500  $\mu\text{m}$ ; (c) example of domain with dominant granular microstructure, in PPL, scale is 500  $\mu\text{m}$ ; (d) rounded aggregate (contoured by red dashed line) in Layer D containing bone fragments and plant matter with a silt capping, PPL and XPL. Note the mainly isotropic nature of the aggregate matrix in XPL, scale is 500  $\mu\text{m}$ ; (e) partially phosphatized limestone grain (ph ls) in sample 406–2 (Layer D, area marked by black square in scan); note also the silty clay capping, PPL, scale is 200  $\mu\text{m}$ ; (f) rare char fragment from Layer D (sample 406–2), PPL, scale is 200  $\mu\text{m}$ ; (g) sand-sized bones, some burned (bb) and coprolite (Cp) Layer D in 406–2, PPL, scale is 200  $\mu\text{m}$ ; (h) photomicrograph of thick, laminated silty sand capping on a limestone fragment, Layer C, PPL, scale is 500  $\mu\text{m}$

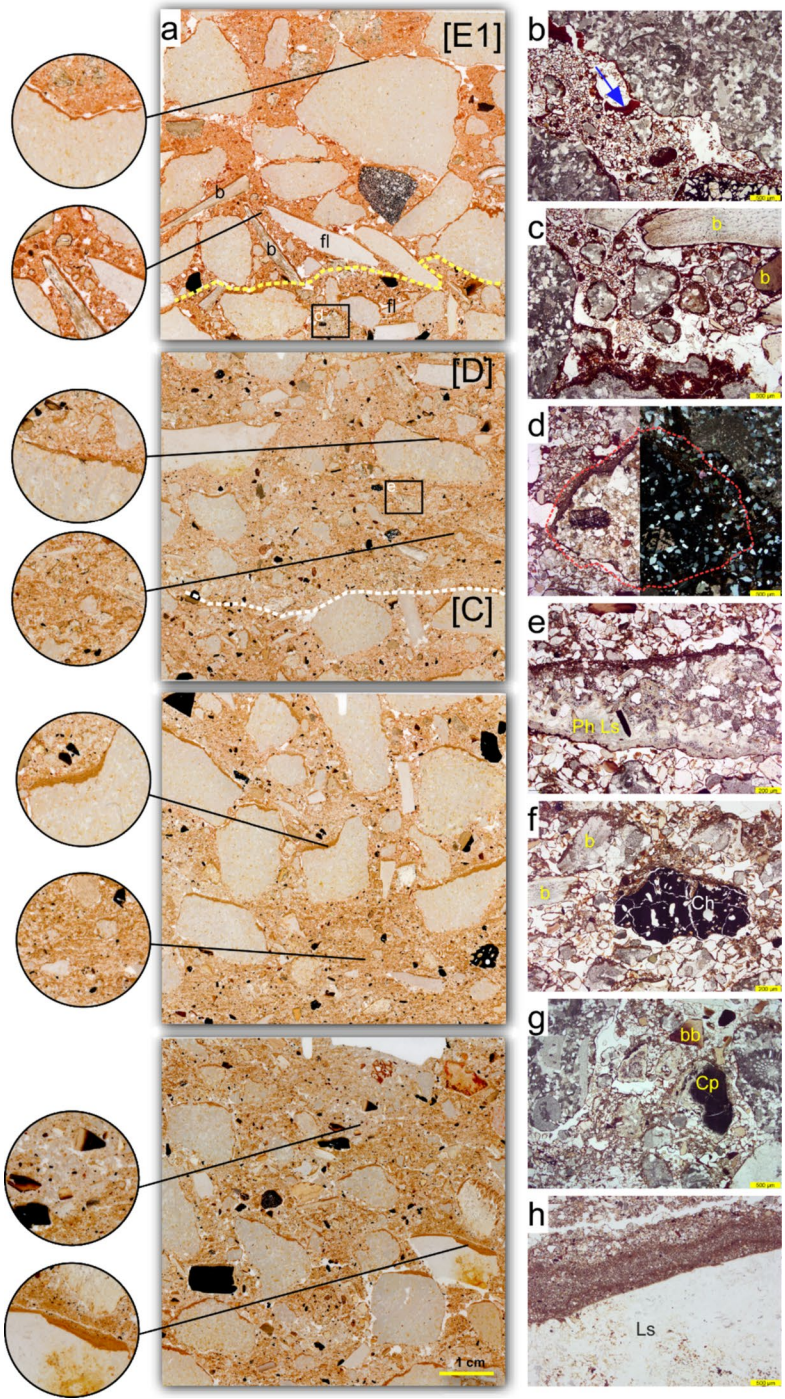
with poorly developed banded fabric. These deposits seem to have been subsequently bioturbated, as shown by the disruption of the banded fabric.

The origin of the phosphatized aggregates remains to be clarified, but they are clearly inherited from somewhere else in the clayey environment. There is an increase in bones, which, as in Layer B, tend to be rounded, often sand-sized, and commonly show traces of burning including some calcined pieces. Interestingly, there are no red iron clay coatings in the lower parts of this layer; however, coatings do appear towards the very top, which seems to be related to post-depositional clay illuviation from the overlying Châtelperronian deposits.

**Layer D (AL LAF8-2).** *Field observations:* This layer varies in thickness from 8 to 10 cm on the E and W walls; on the N wall where it is less eroded by Layer E, it is ~20 cm thick. Layer D reflects a distinct color change, being yellowish red (5YR 4/6), and consisting of sandy silt with limestone clasts having a bimodal size distribution (~1 cm and 4–10 cm). It is a rather uniform band that is inclined ESE and appears to thicken in the direction of the wall constructed by Delporte, i.e., to the S and W. The upper part is comprised of coarser *éboulis* and exposed only on the N face where it is truncated by Layer E1.

*Micromorphological observations:* Layer D is present in one thin section (sample 406–2; Figs. 20 e, f, g), and the deposits are similar to those of Layer C below; they differ from it in terms of relatively thinner cappings on the limestone fragments and partial decalcification of the matrix with domains of coarse monic sand-sized quartz grains. Weak banded fabric is observed at the very top of the thin section, and there are common small bone fragments (some possibly burned) and a fragment of char. Complex phosphatized aggregates, also noted in Layer C, are also present (Fig. 20d).

**Layer E (AL LAF8-1).** *Field observations:* Layer E (~30 cm thick) is a complex of interbedded fine sand, silt, and some clay, stonier at the base; subdivisions of these layers (see below) correspond to Laville and Tuffreau's units L2b2, L2b1, L2a, L2 (from bottom to top) (Delporte, 1984). The base of Layer E (E1) is eroded into Layer D (Fig. 17), and in the field two erosional channels are visible: one on the west side of the section near the wall is ~80 cm wide and about 20 cm deep; it is



filled with Layers E2 and E3 (see below; Fig. 17 b). On the opposite, east side, two broadly defined channels also occur: the one on the N side is ~50 cm wide and ~15 cm deep; the southern one is narrower, ~20 cm wide and ~15 cm deep.

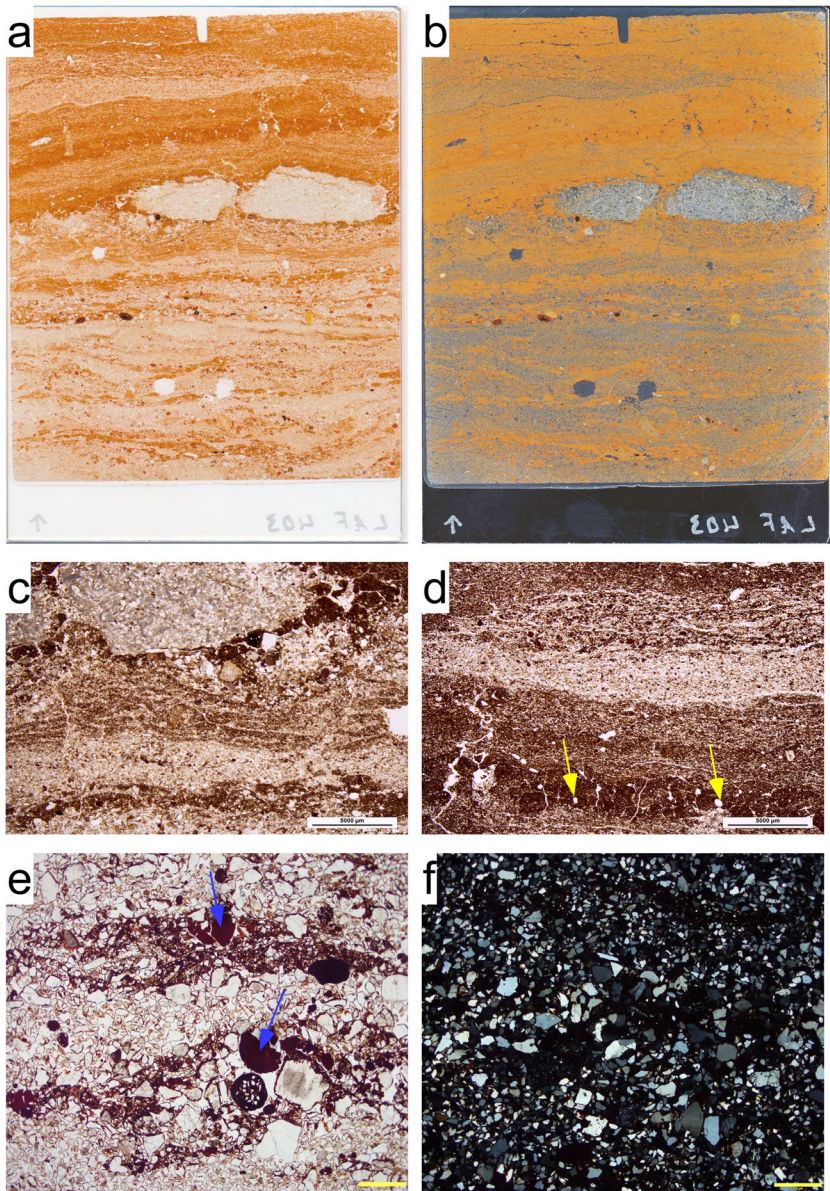
Layer E was subdivided into three subunits (from bottom to top), which have equivalences to Laville and Tuffreau's units:

**Layer E1** (=L2b2 of Laville and Tuffreau) is stony, fine sandy clay. Stones are weathered, and are platy to equant shaped, ~2–5 cm diameter; some reach ~7–10 cm, and they appear to be somewhat more abundant on the eastern side of the trench. Significantly, the limestone clasts are essentially completely coated with red clay, which represents lateral post-depositional percolation of the clay from the direction of the walls of the cave. Overall, however, it is a massive mud-supported deposit with red fine, sandy, silty clay matrix; to the west, the matrix becomes more clayey. Bones are weathered and have yellow-white cores (recrystallized apatite?) when broken.

**Layer E2** (=L2b and L2a of Laville and Tuffreau) overlies Layer E1 with a sharp contact on the N profile. In 3-dimensions, the plane of the contact is generally oriented to the SE and can be traced indirectly toward the SE excavated limits of the site. Layer E2 consists of finely laminated orange sand, and red silt and clay; it exhibits wavy, contorted bedding produced by cryoturbation. It is ~7–13 cm thick. On the E and W profiles, it contains rolled MP artifacts.

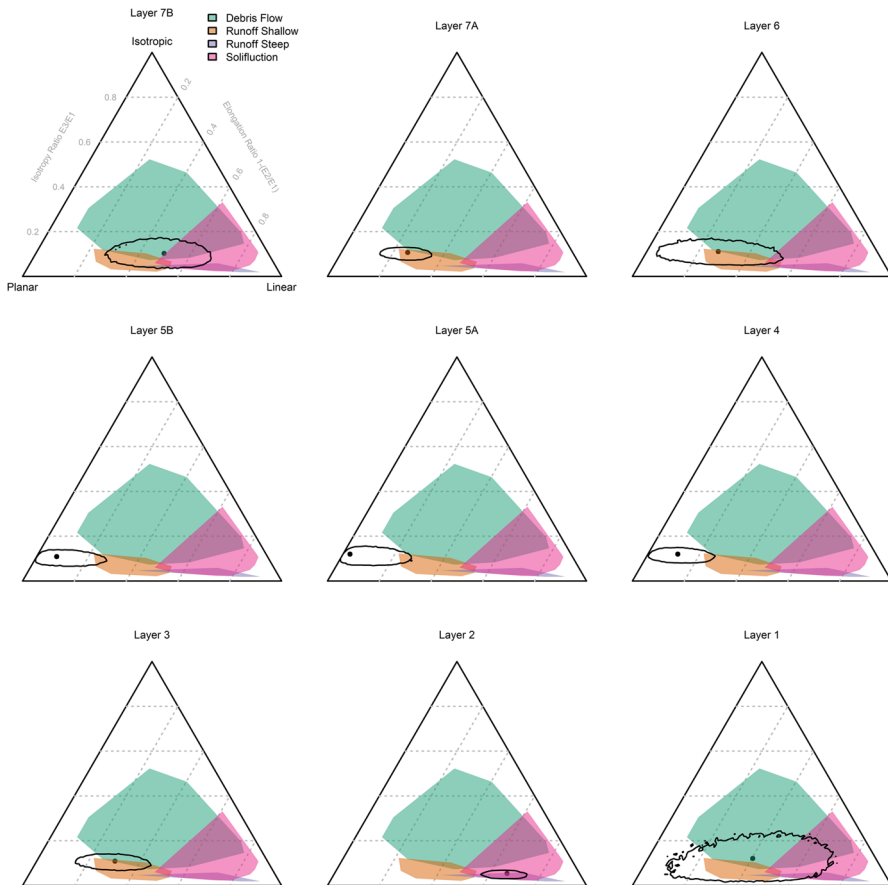
**Layer E3** (=L2a of Laville) is homogeneous and massive clayey silt with platy to laminar structure possibly representing ice lensing and does not show any stratification or graded bedding. Locally contains cm-sized, weathered limestone clasts.

*Micromorphological observations:* **Layer E1**, is very distinct and displays a sharp erosional basal contact as seen in the field. Some coarse burned bones occur in the lowermost 2 cm; bones decrease sharply above (these are not the sand-sized bones as seen below). Phosphatized limestone is also present in this layer. At the very top, banded fabric appears, but in the middle, only cryoturbated grains occur, with complete coatings around them. It appears that some of the clay coatings have been disrupted by the cold. In this layer, we have thick, well-laminated iron-rich clay, which is similar to void infillings. These cold climate phenomena match the cryoturbation described by Laville (2007a, 2007b: 43). Under the microscope (Fig. 21), **Layer E2** shows an alternation of well sorted, finely laminated sands and silts and silty clay lenses. Main components include sub-rounded to sub-angular very frequent quartz grains, few muscovite, common papules of limpid red clay and up to a few cm-size limestone clasts. The groundmass typically varies between chitonic to enaulic in the coarse lenses to close porphyric in the clay-rich lenses. The presence of cryoturbation is clearly expressed with frost-induced microstructures and banded fabric with the presence of vesicles. **Layer E3** is not well represented in the sampled micromorphological blocks.



**Fig. 21** Layer E2 in the Northern Sector. (a–b) scans of sample 403 showing finely laminated silts and sands; (c) detail showing the alternating water laid laminations of silt and clean fine sand, in PPL, scale is 5 mm; (d) similar to (c) but not the clay lens at the bottom with the well-developed vesicles associated with water saturation and drying (yellow arrows), in PPL, scale is 5 mm; (e) details showing the presence of sub-rounded clay papules (blue arrows) and bedded clays, in PPL, scale is 500  $\mu\text{m}$ ; (f) same as (e) but in XPL





**Fig. 22** Benn diagrams for La Ferrassie layers. The dot indicates the calculated values for that layer; the confidence intervals represent a 0.95 based on 50,000 times resampling — adapted from McPherron, 2018

## Fabric Analysis

To assess the degree of movement in the archaeological component of the Western Sector deposits, we look at artifact orientations, lithic breakage, lithic edge damage, and size sorting. The orientation results are shown as Benn diagrams in Fig. 22 (adapted from McPherron, 2018). Most of the layers show a statistically significant preference in bearing angle generally to the southeast in the site grid system (see Table 1 in the Supplementary information). The slope of the deposits, as measured by the plunge angle, is quite consistent and ranges from 9.6 to 13°. When we look at the diagrams in Fig. 22, differences between the layers are more apparent. Including the 95% confidence interval, only Layers 4, 5A, and 5B plot in the portion of the diagram that suggest little movement (the planar corner). The sample size is too small in Layer 1 to know what the orientations are and therefore what the most likely cause might be, but the 95%

**Table 3** Summary of types of cold-climate features from Northern Sector. Tr, traces

Layer	Thin section no	Cappings	Coatings	Infillings	Banded fabric	Rounded grains	Clayey matrix	Notes
E1	403							Bedded silts and clays
E1	406-1	x	x	x		x	x	
D	406-2	x		tr		x		
C	406-3	x		tr		x		
	406-4	x						Washed zones
	407-1	x	tr			tr		
B	407-2	x				x		
	407-3	x	x		x	x		
	408-1	x	tr		x	x		
	408-2	x	x		x	x	x	
A	408-2	x	x		x	x	x	
	410 (mont.)	x		tr		x	x	
	413 (mont.)	tr			x	x	x	
	414	x	x	x	x	x	x	

confidence interval encompasses primarily remobilized deposits. Layer 2 shows the most linearly aligned orientations. Layer 3 is nearer to the planar pole of the diagram, but there is still some alignment consistent with slope movement. The same can be said for the upper Layers 6, 7A and 7B, though the sample sizes are low in 6 and 7B.

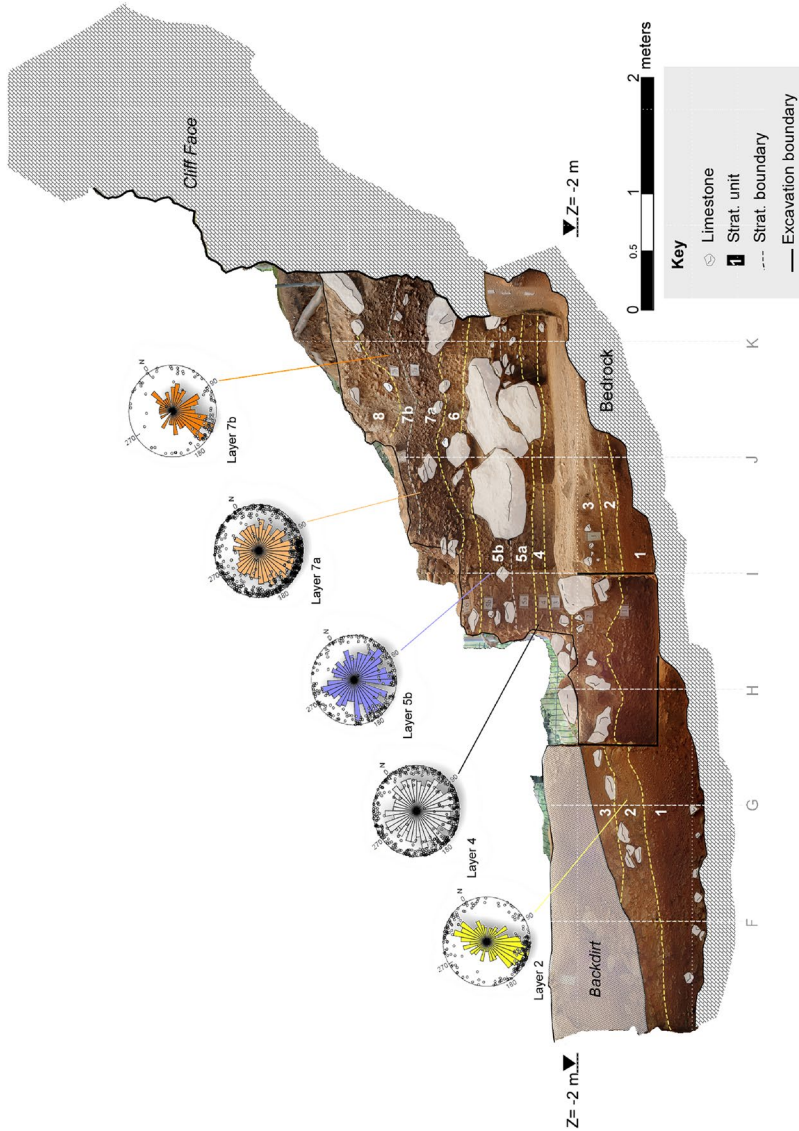
The breakage data are presented in the Supplementary information Table 3. Here, we might expect Layer 2 to show the highest breakage rates (fewest complete flakes), and it does. However, the breakage rates do not differ greatly between layers, and Layer 5A shows approximately the same breakage rate. Based on the breakage data alone, the formation of these deposits seems similar. The Supplementary information Table 4 presents the data on edge damage. Here again, based on the geological observations and the artifact orientations (Fig. 23), we expect Layer 2 to show more damage. In fact, it does, with approximately half of the lithic artifacts showing some damage. In general, there is a separation between the lower Layers 1, 2, and 3 and the upper Layers 4, 5A and 5B with the former showing more damage than the latter. This separation, however, is tempered by the fact that edge damage in Layer 5B is not terribly different from the heavily reworked Layer 2. A comparison of the proportion of small to large finds is shown in the Supplementary information Figure S14 with comparative data drawn from Pech de l'Azé IV. Here, there are no great differences between the layers, though it can be said that Layer 5A has a bit fewer small finds than expected. It is also interesting that, in this regard, Layers 5A and 5B are quite distinct from one another, thus supporting the decision to separate these two deposits in the field. In comparison to Pech de l'Azé IV, the artifact densities and size proportions are similar, and the Pech de l'Azé IV mostly underwent relatively little post-depositional disturbance (Goldberg et al., 2018). The La Ferrassie layers have generally more small finds than the Pech de l'Azé IV layers; however, the difference is small and we looked forward to having more comparative data from sites we excavated in a similar way when these data become available.

## Discussion

### From Cave to Rock shelter

To comprehend better how the site was formed, we consider the origin of the shelter to understand both the formational and topographic relationships of the different parts of the site, particularly between the large shelter (the “*Grand Abri*”) and the Upper Cave located topographically above.

The study of the Upper Cave, located just to the north and west of the large shelter, allowed us to recognize typical karstic morphologies relating to its mode of formation. We observe an interlocking, upward morphology that ends at the top with a vaulted channel. This observation is a good indicator that this cave was formed paragenetically (Palmer, 2007; Jaillet et al., 2009; Lauritzen & Lundberg, 2000; Renault, 1968; Slabe, 1995) (see the Supplementary information), i.e., that it was dug from bottom to top whereby the last stage corresponds to a vaulted channel. This type of genesis is not necessarily indicative of a rising base level but of differential dissolution between the bottom of the cavity and its vault.



**Fig. 23** Orthorectified photograph of the Western Profile facing west showing the identified stratigraphic layers and the Schmidt lower hemisphere diagrams with the superimposed Rose diagram summarizing only the bearing angle distributions. Note that in these diagrams north is in the upper right hand quadrant

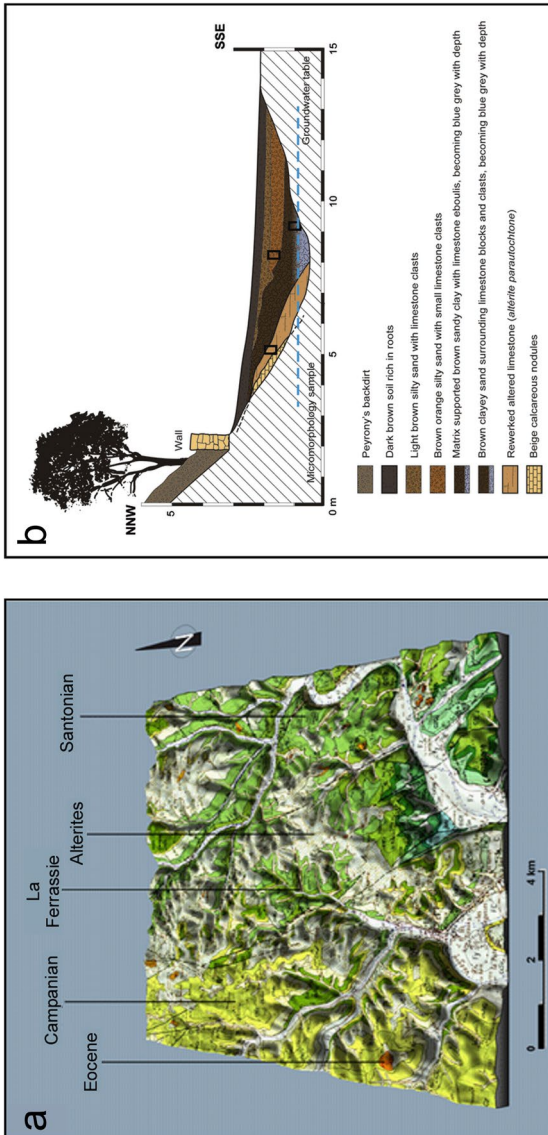
Indeed, when circulating water does not have sufficient energy, insoluble material accumulates on the ground surface. This insoluble fraction thus covers the base of the gallery, which protects the deposits from dissolution, while the vault remains continually exposed. The gallery therefore develops upwards as the base clogs progressively with detrital deposits (mainly sand and clay).

At the regional scale, this process often leads to a reorganization of the karstification and the architecture of the conduits. New galleries may develop higher along the same discontinuity, or they may exploit new fractures, joints, lithological contacts, etc. Commonly, however, the two galleries remain connected by junction galleries (generally smaller), which ensure the circulation of the water between the lower conduit being clogged and the new developing gallery.

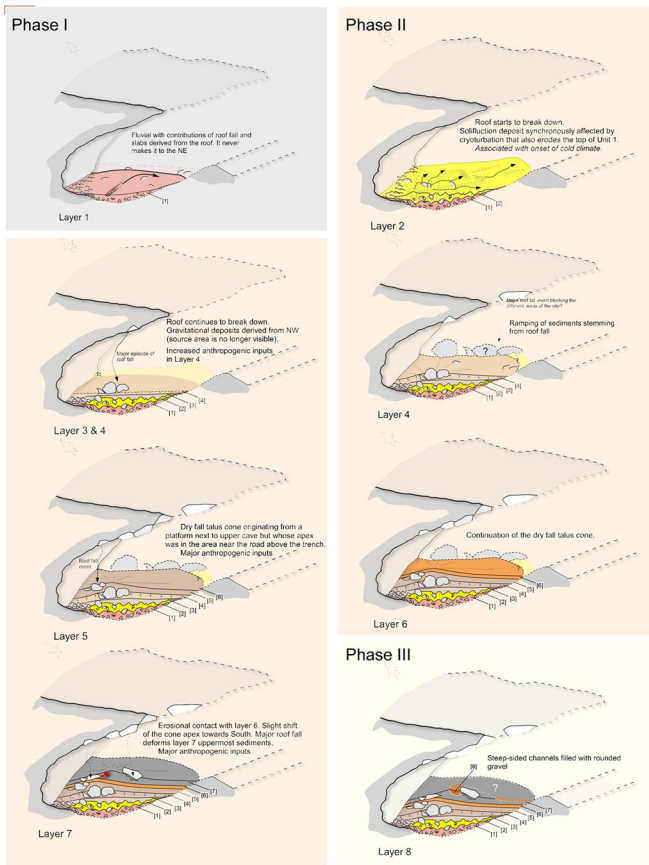
One could recognize this pattern in its broad features at the site of La Ferrassie. The large shelter would correspond to the lower gallery, of which only one wall, largely reshaped since its wide opening, is preserved. The upper gallery (Upper Cave), more confined, has preserved the features of initial paragenetic formation. Several low passages that start at the foot of the south wall of the cave and move towards the large shelter can be interpreted as the connecting drains between the two galleries. While most traces of the other ends of these connecting drains are not visible today in the large shelter, they may simply be covered by the remaining archaeological deposits along the north wall. We have here, in its main features, a typical paragenetic organization.

If the large shelter of La Ferrassie is a simple rock shelter, it should be widely open toward the valley. On the other hand, if it corresponds to a gallery intersected and truncated by the deepening and widening of the valley — as we propose here — we should be able to identify remnants of the base of its southwestern wall. The performed geophysical analyses established that the large shelter corresponds to an old karstic cavity intersected by the topographic surface, rather than a simple rock shelter, which are very common in Périgord valleys. The geophysical profiles (see the Supplementary information) show that the valley now flowing at the base of the site was initially 17 m deeper than it is today and has been progressively filling since the end of the Pleistocene. During these phases of aggradation, the lateral displacement of the fluvial channels attacked the slopes of the valley and hollowed out some of the rock shelters by lateral erosion. Gelifraction also contributed to formation and development by differentially exploiting the more sensitive beds by frost action. One geophysical profile was made along the road passing in front of the site, between the shelter and the dry valley (see the Supplementary information Fig. 2). The computed resistivity model shows that at the site entrance, a highly resistive zone is present, which corresponds to a “rise” of the limestone substrate, as it nearly crops out here. These limestones, which are higher than the lower layers of the sedimentary infilling of the large shelter, do not correspond to the classic feature of a rock shelter. They form a “limestone dam” between the filling of the shelter and the valley and are located in the extension of the vault of the shelter but also at the base of the spur where the cave opens.

If the geophysics revealed the presence of a resistant zone at the southwestern limit of the shelter, it was necessary to verify that it was the calcareous substrate



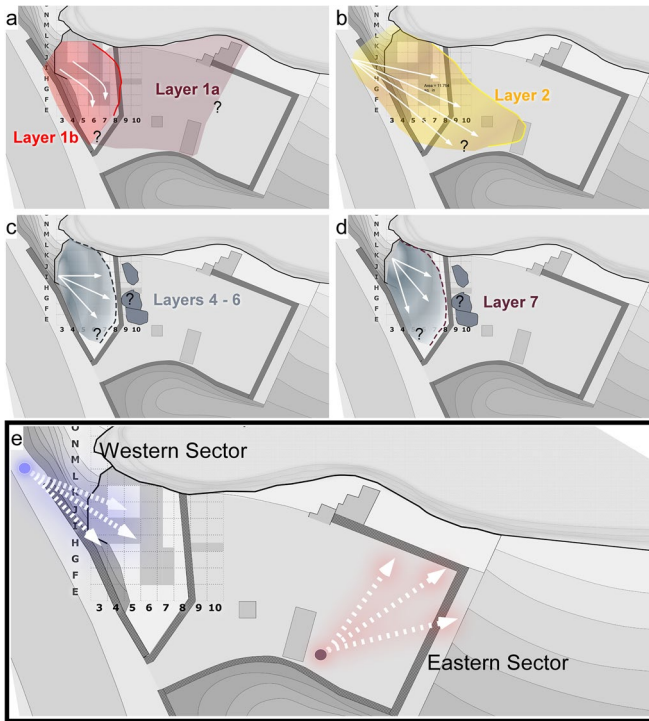
**Fig. 24** (a) 3D model showing the geological and geomorphological context of the site of La Ferrassie (GIS and infography: L. Bruxelles/Inrap); (b) Schematic drawing of the external backhoe trench (see SI for more details) depicting the rise of the cave bedrock to the left of the trench and various kinds of Holocene fills



**Fig. 25** Synthesis of main formation processes in schematic oblique view from above the road and looking towards west. For the spatial extension within the shelter, see Fig. 26 below

and not some collapsed blocks of the vault. So, based on the geophysical results, we made a trench (Trench 4 and labeled “external backhoe trench” in Fig. 2, Fig. 24 and see also the Supplementary information) located outside the shelter, immediately at the SSE of the resistive anomaly, to confirm its origin. In the NNW part of the trench, a few decimeters deep, we reached a cream-colored, nodular limestone exactly where it had been indicated by geophysics. The dip, the lithology, and the morphology of the outcrop confirmed that this was the local Coniacian limestone substrate, and, in fact, it is nearly cropping out under the current access gate to the site and directly supports the south fence wall. Sloping about  $20^\circ$  towards the bottom of the valley, it is covered by a variable thickness of alterites and limestone clasts (colluvium) containing reworked lithic archaeological material.

Our interpretation is that, due to climatic variation during the Quaternary and resulting alternations of incision and clogging of the valley bottoms, the valley slopes underwent successive phases of erosion which eventually truncated and



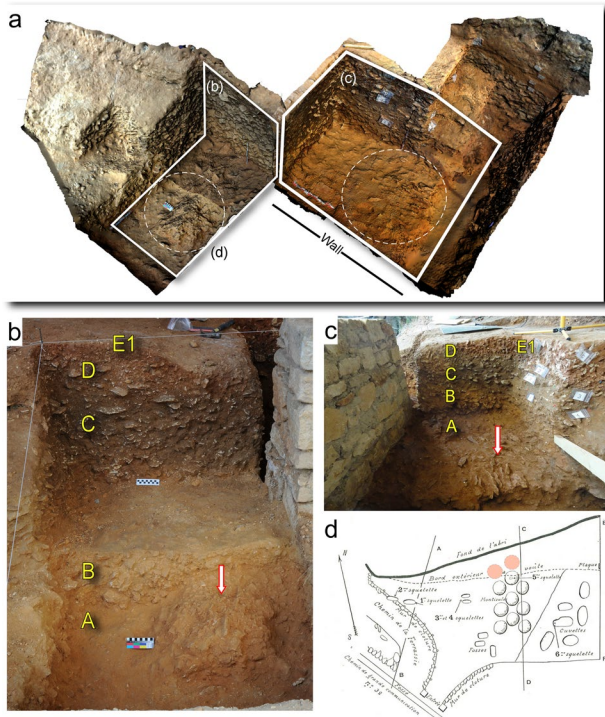
**Fig. 26** Schematic view of inferred extension of Western Sector layers (**a** to **d**) towards East; (**e**) Direction of sedimentary sources with the apex of the depositional cones for the Western Sector shown in purple and those previously established (Bertran et al., 2008a; Texier, 2009) for the Eastern Sector shown in red. Note that these distinct sedimentary sources result in different depositional histories across the extension of the La Ferrassie site

breached the southwest wall of the cave but left behind a portion of its base. This remnant wall of the gallery played an important role in the formation of the site as it acted as a sedimentary dam behind which the colluvium and archaeological deposits were preserved; the deposits inside the footprint of the large shelter avoided being eroded into the valley. Only deposits protected in cavities or shelters like these tend to have been preserved in the region.

### Sedimentary Dynamics and Formation Processes

Based on our recent excavations, field descriptions coupled with micromorphological, and fabric analysis have allowed us to propose the main site formation processes, which are synthesized in Figs. 25, 26. Here, we will focus on the most prominent evidence for reconstructing such processes and compare the available new data with previous research at the site.





**Fig. 27** View of stratigraphy and stony features in the North Sector. **(a)** 3-D model of excavations of the North Sector. White solid lines depict the location of the photographs shown in **b** and **c**, whereas the dashed white circles show the location of the two stony feature (monticules) found during excavation, scale is 10 cm wide at left and 50 cm at right; **(b)** Field view of the stratigraphy looking North, showing layers and one of the monticules (arrow), scale is 10 cm wide; **(c)** Field view of the stratigraphy looking West, showing layers and another monticule feature (arrow); **(d)** Schematic map of Peyrony (1934) with the location of the monticules, Neanderthal skeleton and other features where we added the two new identified “monticules” in the Northern sector shown in red

## The Western Sector

Albeit a relatively small area, establishing the nature of site formation in the Western Sector is particularly complex due not only to inherent sedimentary dynamics, but also because this area had substantially changed since the initial excavations by Capitan and Peyrony — for which there is scant documentation by today’s standards. Similarly, these deposits were partially truncated towards the south and east during these early excavations and back dirt, presumably resulting from Capitan and Peyrony’s excavation moving progressively eastward, is found directly atop Layers 3 and 2. Overall, the lithology of the deposits in the Western Sector are variable, but they do change markedly from bottom to top. We can summarize the sedimentation dynamics into three main phases where: phase I corresponds to fluvial processes associated with Layer 1 deposits, phase II is linked to slope processes and, although important differences exist among the layers (discussed below), and includes Layers

2–7; finally, phase III is linked to channeled deposits of Layer 8. Due to the limited exposure of Layer 9 deposits, these will not be discussed here.

**Phase I (fluvial sedimentation):** Overall, the deposition of Layer 1 at the base of the sequence represents a combination of water deposition likely related to meandering of a small channel in the main valley to the south, combined with local contributions of limestone roof fall and gelifracted clasts along the northern limestone wall of the large cave/shelter. Specifically, the weakly bedded quartz-rich sands and silts, which commonly contain iron-rich clasts, point to water deposition. This inference is supported by the localized occurrence — particularly near the upper part of the layer — of elongated small channels, enriched in these iron-rich clasts (Fig. 7c). The iron clasts also indicate their reworking from older soils located on the plateau and on slopes in the site environs. In any case, the channels have a NW–SE orientation and are inclined to the SE indicating flow in this direction. These localized channels or bedded sands do not appear to extend inside the cave system, as these types of sediments were not encountered in any of our test trenches (see the Supplementary information for more details), nor in the profiles from Delporte’s excavations. They probably indicate runoff from the slopes that was confined to the area of our excavations in the Western Sector.

On the other hand, the remainder of the sediments of Layer 1 are enriched in subangular to sub-round limestone clasts that presumably derived from the roof but also from the slopes just north of the entrance, where they have been somewhat rounded by weathering and downslope processes. In contrast, along the northern wall of the large cave/shelter, the presence of angular to sub-angular bedrock slabs corresponds to local cryoclastic weathering of the bedrock floor and wall. The dates of Layer 1 (Table 2) suggest that it accumulated around MIS 5 but there is nothing inherent sedimentologically to indicate a specific climate.

**Phase II (cryoturbated slope deposition followed by colluviation):** Sedimentation dynamics change drastically from the time of deposition of Layer 2 onwards. Microscopic examination reveals that Layer 2 deposits are composed mainly of calcareous silts and sands that display a well-developed banded fabric along with common cappings. These micromorphological characteristics point to solifluction and cryoturbation. An association with cold climate is corroborated by field observation and orientation analyses. Indeed, the linearly aligned orientations of Layer 2 artifacts are consistent with the solifluction processes for this layer. In McPherron (2018), we also noted that the northeastern portion of this deposit shows fewer linearly aligned artifacts than in the southwestern portion. The artifacts of this layer also show the highest breakage rate and a low percentage of artifacts with no edge damage. The evidence suggests that Layer 2 represents essentially pulverized and decomposed limestone produced and transported under cold climatic conditions by solifluction, a slow downslope creep process (Rowley et al., 2015). The cold climatic environment existing at the time of Layer 2, which partially affected the underlying Layer 1 deposits, is associated with MIS 4, with an OSL age between  $74 \pm 5$  and  $62 \pm 4$  ka (Guérin et al., 2015). Layer 2 increases in thickness to the WNW, and thins and eventually disappears to the east, as previously recognized by Peyrony (Delporte, 1984). A thin lens of it was identified in our Trench 2 (see the Supplementary information), likely marks its easternmost extent. The source of

Layer 2 must be tied to a knob of limestone bedrock or heap of boulders that existed in the area of the current Departmental Road (see Fig. 2) approximately in the area of squares F2, G2, H2. This was likely roof fall near the then western-most location of what was the cave mouth that extended out at least this far in Layer 2 times, as is supported by the existence of very large (several-meter sized) boulders that topped the later deposits in this area. These boulders were since removed but they can be seen in historic photographs of the site (in Capitan & Peyrony, 1912 see Figs. 2 and 3). By the end of the deposition of Layer 2, the Western Sector area had an uneven, undulating surface resulting from the different solifluction lobes.

The sequence of deposits overlying Layer 2 — Layers 3 to 7 — are overall similar, with minor differences in composition and archaeological content. They generally consist of poorly sorted, coarse to medium silty sand with increased presence of bones, lithics, limestone clast from roof fall and local contributions of cm-sized rounded gravel coming from the slopes as in Layer 8 (see above). Layer 3 and the basal sediments of Layer 4 tend to be more tabular, and they fill in the topography of the underlying Layer 2. They represent occupations that punctuate accumulations of stony and muddy deposits over a 6-m surface with a very low slope (2°). By the end of Layer 3 time, we note the onset of decalcification of the limestone fragments along with thicker dusty clay coatings. There is no evidence for running water or sorting, and the depositional processes result from gravitational accumulation concomitantly associated with limestone breakdown. In fact, the artifact orientations from Layer 3 are consistent with some downslope movement, though from a lithostratigraphic point of view these non-planar orientations result from these deposits infilling the underlying uneven topography of Layer 2. The radiocarbon chronology reported in Talamo et al. (2020) points to an age inversion in Layers 4 and 5 with a ~2000 years difference. However, and as discussed in-depth (Talamo et al., 2020), this age inversion is difficult to envision from a stratigraphical and site formation point of view, as it would entail Layer 5 being deposited somewhere above the site and reworked, while maintaining internally consistent dates. The artifact orientation of the artifacts from Layers 4 and 5 is consistent with intact deposits. The accumulation of the upper part of Layer 4 through to Layer 7 relates to deposition of sediment along an ever-increasing slope (up to ~5° in Layer 7). The slope is in part dictated by the relief produced by the accumulation of large blocks of roof fall at the presumed entrance (along squares ~I/J/K 3–4) where we see evidence for continued accumulation of large roof fall blocks during Layer 2 times and the progressive collapse of the immediate roof mainly from the time of Layer 4 onwards.

While no ashes were observed, burned bones and char fragments are commonly observed with spatially discrete concentrations of burned bones (some calcined) occurring particularly in Layers 3 and 4. These concentrations are interpreted as poorly preserved remnants of combustion features. Their disruption and poor preservation are probably related to trampling and the location of these features on a slope giving access to the Upper Cave area.

Though the archaeological materials in Layers 4 to 7 are not strongly aligned, they do conform to the slope of these deposits (roughly to the SE) and appear to be related mostly to sliding of the geological and archaeological material down a radiating

slope, although some evidence of rotation of grains can be seen in thin section (e.g., Fig. 14) (see Karkanis, 2019). Despite this, the artifacts from these layers show the highest rates of undamaged pieces and high rates of complete artifacts. Elements such as the poorly sorted nature of components and the frequent presence of calcitic grains (silt- to granule-sized) point to gravitational fan-like accumulation with mechanical limestone disaggregation in conjunction with dm-sized roof collapse in what would have been the westernmost part of the roof. As viewed in the field, and coupled with fabric analysis, the deposits indicate a continual source area to the NW or WNW, with the apex of the cone estimated to have been located some meters south of the Upper Cave terrace. This extended terrace was likely destroyed by the construction of the Departmental Road. The apex of the cone apparently shifted slightly northward during Layer 7 times, when the slope had become steeper and more marked (this is seen as well in the artifact orientations which indicate a more linearly oriented fabric). Taken together, successive episodes of roof fall at the cave entrance at the time resulted in the accumulation of masses of limestone. This massive accretion not only produced a topographic high spot and source of limestone-rich sediment, but also effectively restricted the living and circulation area in the Western Sector. In general, whereas occupations took place on these slopes, a significant amount of the sediment originated upslope in the direction of the fan apex on the platform that must have extended out from the terrace of the Upper Cave. It is there that we infer more pronounced occupations took place, with occupational debris being displaced and moving down the slopes of the cone. Therefore, we can expect that part of the lithic assemblages underwent short-distance displacement in the Western Sector.

Finally, in terms of post-depositional processes, a marked lateral variation in the Western Sector occurs, as all the deposits along the cave wall to the north have been strongly decalcified. This post-depositional process results in a substantial loss of volume (up to ~30–40%). It includes post-depositional decalcification of limestone fragments and concomitant release of unbleached quartz grains derived from the bedrock. The effects of this dissolution have consequences for OSL age determinations, as already discussed in Guérin et al. (2015).

**Phase III (channeling):** Layer 8 is composed of bedded, cm-sized rounded gravel infilling channels that cut into the underlying depositional cone. The deposits have no fine matrix and artifacts are rare. They represent water laid channelized flows originating from the area near the entrance to the Upper Cave that rework decomposed gravels.

### The Northern Sector

Excavations in the Northern Sector were spatially limited and focused on cleaning small (~60 to 70 cm thick) profiles left by Delporte's excavations in the 1960s and 1970s. Any Aurignacian deposits that might have existed here were removed by Delporte and what remains are distinct laminated silts and clays with mixed assemblages (Delporte, 1984) laying atop Mousterian deposits. The stratigraphy exposed in the profiles was partly described by Laville and Tuffreau in Delporte (1984). In this area, we were able to construct a stratigraphic sequence subdivided

into five main stratigraphic units based on a few clean views in our restricted excavations, along with extant profiles. Given our spatially restricted excavations and the lack of lateral visibility, our inferences relating to the sedimentary dynamics are limited. Thus, only the most prominent aspects are discussed here and, where possible, integrated with results from previous geoarchaeological investigations.

Overall, the bulk of the deposits exposed here consist of limestone clasts derived from the roof and walls, small bone fragments, silty clay matrix, and common laminated red silt and clay cappings on the clasts (Fig. 17). The basal deposits, Layers A and B, are strongly affected by cold features (cappings and banded fabric) and the formation of these specific layers is further explored in the “[Periglacial Features: Peyrony’s monticules and the implications for the context of the LF8 skeleton](#)” section below.

The specific depositional processes for most of Layers B, C and D are difficult to address given our limited visibility of the deposits in our excavated squares and their lateral continuity. It is, however, relevant to indicate the distinct orientation of these layers: Layers B and C dip to the NW. Unit D, on the other hand, is inclined to the ESE, and is thicker to the S and W, being truncated by the Layer E1 above. These distinct inclinations point to a change in the sedimentary sources. Note that some of our stratigraphic descriptions are strongly at odds with some of the data presented recently by Balzeau et al. (2020). They describe, for example, that the bones of the Neandertal infant (La Ferrassie 8) recovered from this location by Delporte, are inclined in a different direction from that of the surrounding sediments at the same elevation. Our work clearly shows that this is not the case: the bones and the deposits are inclined in the same way (see below).

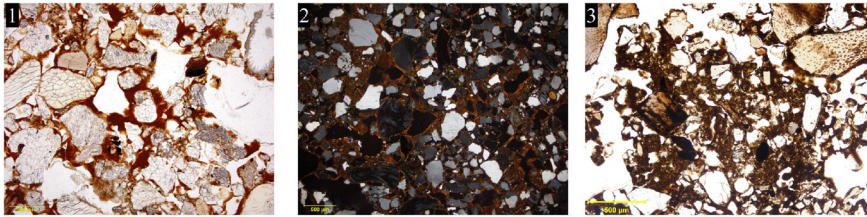
Although there is a very low density of artifacts, the abundance of sand-size fragments of burned bone is clear in thin section, as is the presence of complex phosphatic-rich rounded aggregates. The ultimate origin of these components remains a mystery, but they speak to the reworking of previously deposited archaeological deposits from elsewhere in the site complex. Similarly, Texier (2009) notes the abundance of ‘tiny’ [sand-sized] fragments of burnt bone — some bedded — that they attribute to reworking by runoff and frost-related phenomena (e.g., solifluction, cryoturbation) (Texier, 2009, p. 97). Although they could relate these small burnt bone fragments to what might have been combustion features on the Eastern Sector (*coupe sagittale*), we were unable to locate any such features during our limited excavations in the Northern Sector.

Finally, the deposition of Layer E marks not only a cultural change (with the inclusion of Châtelperronian elements) but also a significant sedimentary one. This change is clearly demonstrated by channeling and the accumulation of sheetwash deposits that are readily discernable both in the field (erosive channels that cut into the underlying Layer D) and under the microscope (well-sorted and finely laminated silts and sands). These deposits were subsequently affected by cryoturbation, as previously observed by Laville and Tuffreau (Laville & Tuffreau, 1984).

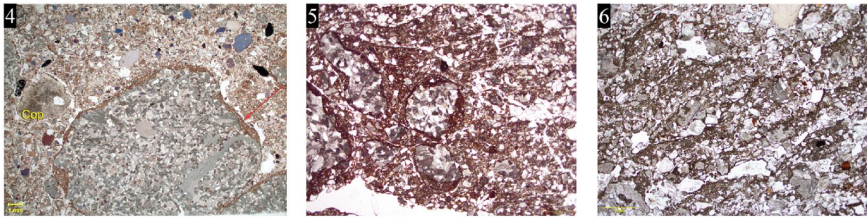
## Description

**Coatings** (Photos 1-3) are present either as poorly sorted brownish red, dusty silty clay coatings with-in pores, particularly between grains; or as dark red limpid, laminated coatings in voids.

The dusty coatings are present from Layer 3 onwards and appear to be syn-depositional. The limpid coatings tend to be a late stage event and, though they are present elsewhere, are particularly abundant near the cave wall.



**Cappings** (Photos 4) are dominant in Layer 2 and are comprised of massive and laminated calcareous silt and fine sand. These cappings are associated with cold conditions during and after Layer 2 times and partially affect uppermost part of Layer 1.



**Banded fabric** (Photos 5-6) is characteristic of Layer 2 in the Western Sector and in Northern Sector sediments. Associated with cold events and ice segregation.

**Fig. 28** Examples of cold affected deposits under the microscope

### Periglacial Features: Peyrony's Monticules and the Implications for the Context of the LF8 Skeleton

One of the most striking aspects uncovered in the Northern Sector is the presence of cryoturbation features throughout most of the exposed sequence and, in particular, two stony features encountered at the base of the sequence (affecting Layers A and B) that are similar to what Peyrony (1934) described as *monticules* [but see also Laville (2007b)]. In the field, these features consist of concentrations of limestone fragments approximately 50–70 cm in diameter that have a domed appearance in which the platy clasts are oriented sub-vertically (Fig. 27). Under the microscope, laminated silty clay cappings are ubiquitous and poorly developed banded fabrics are localized in the bottom of the profile (Table 3; Fig. 19 and 28). These formations are consistent with well-described patterned ground features (e.g., Bertran et al., 2010; Masson, 2010) and are indicative of freeze–thaw conditions involving the frost-jacking of limestone clasts in a flat area (Bertran et al., 2010; Van Vliet-Lanoë, 1991). Peyrony originally interpreted these formations as part of a cm- to dm-thick undulating relief that was of anthropogenic origin and associated with the La Ferrassie 5 remains (Laville, 2007a, 2007b). In contrast, our field and microscopic

evidence attests to the natural origin of these *monticule* features as well-known geological phenomena — in contrast to Peyrony's interpretation. One of these monticules was situated underneath the find location of the La Ferrassie 8 Neanderthal remains (Balzeau et al., 2020; Delporte, 1984; Gómez-Olivencia et al., 2015).

It is interesting, however, that practically the entirety of the overlying deposits in the Northern Sector displays cold-related features (Table 3, Figs. 19 and 20). Virtually all layers exhibit some extent of cold post-/syn-sedimentary signatures, with red silty clay cappings on coarse components (e.g., limestones, bones, and phosphatic aggregates), and rounded limestone grains, including cryoturbated and rotated grains. However, only the lower layers, A and B, display well developed banded fabrics and patterned ground formation, which would suggest a more extreme periglacial environment. The continued evidence for cold climate features through Layers C-E in the Northern Sector is strikingly different from what we observed in the Western Sector where none of the layers above Layer 2 exhibits such microscopic and macroscopic cryoturbation-related evidence.

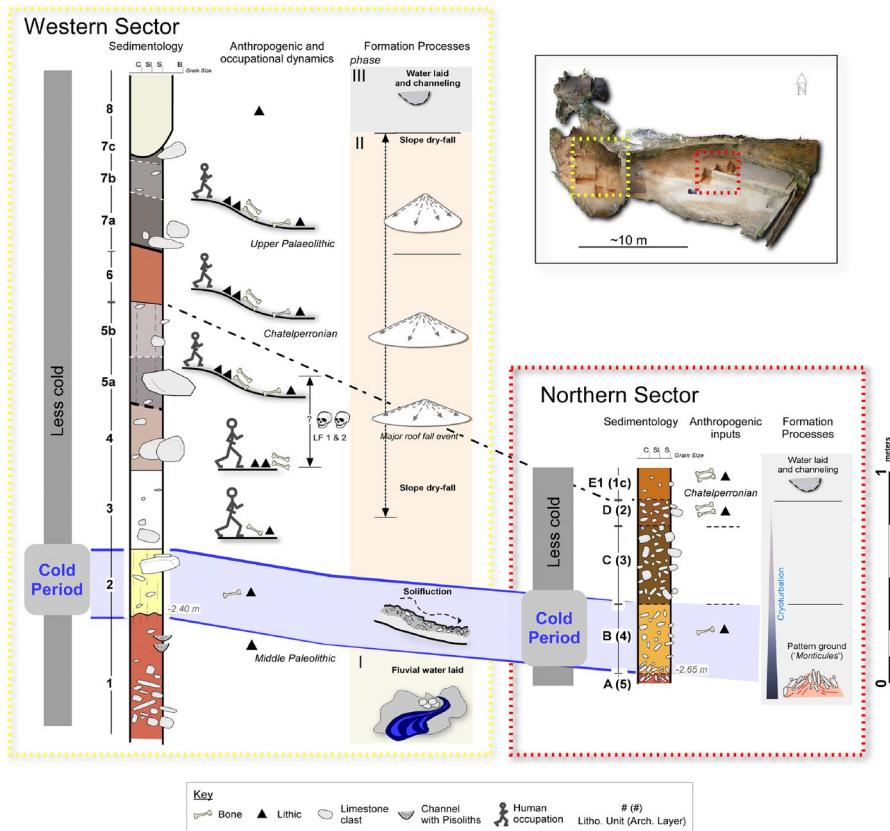
We interpret the longer physical and temporal span of cold climate features in the Northern Sector deposits to be related not to global climatic fluctuation, but to different microenvironments within the site. Specifically, while the Western Sector was essentially at the cave mouth, the Northern Sector was deeper inside the cave and a colder microclimate in this interior part of the cave could result from cold air continually draining into it from the exterior. The reconstructed morphology of this area during the accumulation of Layer A-E would be that of an old karstic gallery truncated on its southwestern side by the valley. In the geophysics results, confirmed by the deposits exposed in the external backhoe trench (see Supplementary information Sect. 2.4 for more details), we identified the presence of a remnant of the southwestern wall, which separated the cave from the valley.

The geometry of the layers in the Northern and, more clearly, on the Eastern Sectors (Bertran, 2012; P. Bertran et al., 2008a, 2008b; Delporte, 1984; D Laville, 2007a, 2007b, Texier, 2009) implies the presence of an accretion talus that sloped towards the NE. This geometry would imply that cold air would flow from the cave's entrance, along the talus and accumulate at its base along the north wall of the cave. This would essentially function as a cold air trap. This means that even if outside the cave, the climate was temperate enough that the soil could daily thaw, within the cave, cold air was accumulating, with seasonal frost deeply affecting the deposits.

Therefore, in our reconstruction, the morphology of the shelter had a strong influence on microenvironments within the site, with marked localized colder conditions inside the cave in the Northern Sector, but also Eastern Sectors (see Bertran, 2012; Bertran et al., 2008a; Delporte, 1984; Texier, 2009) when compared to the more exposed deposits in the Western Sector presented here.

### **Distinct Sedimentary Histories Across the La Ferrassie Large Shelter**

As noted previously (Bertran et al., 2008b; Texier, 2006) the history of La Ferrassie encompasses a complex of sedimentary sequences, with several sedimentary sources. This is particularly true when we consider not just the Western Sector, but also the



**Fig. 29** Synthetic depiction of the stratigraphy in the Western and Northern Sectors of La Ferrassie, with the inferred climatic associations, preferential locations of human occupations on and above the slope, main formation processes and inferred penecontemporaneity between the two areas

deposition in the Northern and Eastern Sectors. Unfortunately, the > 10 m-wide swath of deposits that would have linked the Northern and Eastern Sectors with the Western Sector was largely removed by Capitan and Peyrony and today little information is available on the characteristics of these deposits. Consequently, there is no direct stratigraphic correlation between these areas of the site. As we have described above, the types of sediments and their formation processes are quite different.

Despite the lack of physical correlation, however, the formation of patterned ground features in Layers A and B in the Northern Sector is likely contemporaneous and roughly coeval with the solifluction deposits of Layer 2 in the Western Sector (Fig. 29); both stand out as marked evidence of colder periglacial conditions. These types of cold-related deposits express different periglacial features, one developing in a slope (Layer 2) and the other in a flat surface (Layers A and B). The two OSL dates for Layer 2 ( $62.5 \pm 4.0$  and  $74.2 \pm 4.6$ ) (Guérin et al., 2015) and OSL dates for



Layers A and B in the Northern Sector ( $67 \pm 4$  and  $60 \pm 7$ ) (Balzeau et al., 2020) indicate general contemporaneity and an association with cold MIS 4.

For the Western Sector, our geoarchaeological investigations show that the majority of the deposition (with the exception of Layers 1 and 8) is related to sedimentary cones emanating from a topographic high situated to the NW, that is, situated roughly where the Upper Cave terrace meets the current Departmental Road. In contrast, as discussed by Texier (2009a), this type of ‘cone sedimentation’ was also noted in the interior of the cave (Northern and Eastern Sectors), but the apices and depocenters of these distinct cones shifted with time from west to east. Therefore, for most of its sedimentary history, we must envision several sedimentary cones contributing to sedimentation in the different areas of the La Ferrassie complex.

In sum, evidence for distinct depositional cones and the lack of lithological similarity between the Western and Northern Sectors, and what is visible in the Eastern Sector as left by Delporte, demonstrates that La Ferrassie is not just one simple locality but several distinct loci of deposition. Each one appeared to have its own, independent sedimentary sources and, potentially, human occupations.

## Conclusions

One-hundred years of research at La Ferrassie demonstrate that the sedimentary history is complex and variable within the site’s space. In this paper, we presented new data based on recent excavations on the Western Sector of the site and observations based on limited excavations of the Northern Sector.

Our site formation data show that, throughout most of its occupation, La Ferrassie was effectively a rock shelter, although geomorphologically the site complex is part of a cave system that continues beyond the excavated area and Mousterian occupations towards the East were located inside a cave setting. This evidence indicates that the entrance of the cave was in the area of the Western Sector and that during initial Middle Paleolithic occupations the site was a large, partially roofed cave that continued towards the east. The breaching of the southern wall occurred early on, and continued roof collapse occurred throughout the Upper Paleolithic sequence. This is apparent in our Western Sector but is most clearly seen in the large profile left by Delporte’s excavation in the Eastern Sector (Delporte, 1984).

The combined evidence from our excavations and those from previous work at the site by both Peyrony and later Delporte leads us to interpret La Ferrassie not just as one large site but rather a complex of distinct depositional zones that had distinct, and often independent, sedimentary histories. Sedimentation sources and processes differ substantially at the cave’s entrance (Western Sector) versus the inner areas (Northern and Eastern Sectors). Each of the loci has a different depositional and post-depositional history with implications for reconstructing human occupations at the site. Some of the more relevant depositional and post-depositional aspects can be synthesized as follows:

- The Western Sector sequence is characterized by a succession of depositional environments: Phase I of fluvial sedimentation (Layer 1); Phase II of solif-

lucted and cryoturbated slope deposits (Layer 2) and accretion cones (mainly from top of Layer 4 upwards); and a Phase III associated with localized water laid channels (Layer 8).

- The Northern Sector sequence shows the presence of patterned ground affecting limestone clasts and matrix at the base of the deposits. These features were previously described as *monticules* and interpreted by Peyrony as anthropogenic in origin. Here, we show the natural (geogenic) nature of these deformations related to periglacial climatic conditions.
- There are distinct orientations of the layers in the Northern Sector, with Units B and C dipping to the NW whereas unit D is inclined to the ESE, indicating a change in sedimentary sources between these layers. The inclinations of the lower layers to the NW are in agreement with the overall inclination of the Neandertal remains of LF 8 and not at odds with it as suggested by Balzeau et al. (2020) to indicate that the LF 8 skeleton was purportedly interred.
- The morphology of the shelter had a strong influence on microenvironments within the site, with marked colder conditions inside the cave, that is, along the Northern and Eastern Sectors, when compared with the more exposed Western Sector. In the Western Sector, there is no evidence for cold-associated signatures during the Upper Paleolithic and Châtelperronian occupations. On the other hand, the presence of gelifraction, ice lensing, and platy structures shows that cold conditions clearly affected all the deposits in the Northern and Eastern Sectors.
- The main post-depositional process we observed relates to preferential decalcification of the sediments near the back (north) wall in the Western Sector. This process results in a loss of volume and the post-depositional release of angular quartz grains from limestone clasts into the deposits — which, in turn, has consequences for dosimetry estimations for OSL dating of these sediments (Guérin et al., 2015). In the Northern Sector, bioturbation by small soil fauna affects the exposed deposits of Layer C and syn- and post-depositional cryoturbation affects all the layers in this area.

Taken together, the suite of depositional processes has implications for interpreting the integrity of the embedded archaeological assemblages and inferences on the primary location of human occupations. Generally, while occupations occurred in the area of the Western Sector, a notable portion of the sediment originated higher up in the direction of the fan apex on the platform of the Upper Cave. This is where we believe more extensive occupations took place with occupational debris being syn-depositionally displaced down the cone's slope over short distances. We can synthesize the main points as follows:

- The water-lain deposits of Layer 1 resulted in reworking of the (rare) archaeological material found in this layer.
- For Layer 2, the soliflucted and cryoclastic/soliflucted nature of the sediments involves reworking of archaeological material from relatively nearby occupations to the NW. This is also shown by the fabric analysis with linearly aligned orientations of the artifacts and high breakage rates, with few complete flakes.

- Middle Paleolithic Layer 3 and the base of Layer 4 do not show substantial reworking of the archaeological material, and it can be inferred that occupations were at or close to the excavated area. This is also shown by the presence of discrete burned bone concentrations, albeit poorly preserved.
- At the end of deposition of Layer 4 and throughout Layers 5 (Middle Paleolithic) and 6 (Châtelperronian), continued roof fall events may have restricted the occupation of this area; occupations shifted more to the upper cave terrace above the excavated area, with likely downslope movement of archaeological materials.
- The accentuation of the depositional cone during Layer 7 (Upper Paleolithic) implies that the bulk of human occupation was probably located on the upper cave platform, with sliding of artifacts along the slope towards the Western Sector area.
- Finally, the water-laid deposition of the spatially restricted uppermost part of Layer 8 deposits shows that any (rare) artifacts would have been reworked and redeposited at this location.
- Neanderthal occupations seem to have been more extensive towards what was the front/exterior of the cave (Western Sector), with lower artifact densities reported from the Northern Sector. While the large central area excavated by Peyrony yielded many artifacts (Dibble et al., 2018a, 2018b), the lack of spatial data for these old excavations hampers our understanding if these artifactual concentrations were equally spread throughout the entire excavated area or, for instance, closer to our Western Sector.
- Upper Paleolithic occupations seem to have been dispersed throughout the (E-W) length of the site complex; this is particularly the case in the Western and Eastern Sectors, as well as on the platform in front of the upper cave.

A complete understanding of a large and complex site such as La Ferrassie is challenging. A difficult aspect of this study is that so many pieces of the puzzle were removed by excavation early on, and there is little or no data available to us today on the deposits and site configurations in these excavated areas. In this sense, we were forced to do a bit of the archaeology of the archaeologists. Recording not only the artifacts, but also their sedimentary context — the backbone and major constituent of the archaeological record — is a crucial part of any modern archaeological enterprise. We should strive to improve this situation for future generations researching the sites that we are digging today.

**Supplementary Information** The online version contains supplementary material available at <https://doi.org/10.1007/s41982-023-00159-7>.

**Acknowledgements** This paper is dedicated to the memory of our colleague and friend Harold Dibble. Harold was an outstanding scientist, a brilliant mind, and a true inspiration to all who knew him. His lead and contributions to the work at La Ferrassie presented here were invaluable. We are very appreciative for the reviewers' efforts to help us improve this lengthy manuscript.

**Author contribution** Conceptualization: V.A., P.G., A.T., D.S. and S.M. Excavation permit: A.T. Field sampling and stratigraphic descriptions: V.A, D.S, P.G. Micromorphological analysis: V.A., P.G. Fabric analysis: S.M. Geomorphology and Geophysics: L.B. Writing, review, and editing: V.A., P.G., D.S., S.M., A.T. All authors reviewed the manuscript.

**Funding** Open access funding provided by FCTIFCCN (b-on). Work at La Ferrassie from the Leakey Foundation, Max Planck Society, Ministère de la Culture (Service Régional de l'Archéologie, Musée Nationale

de Préhistoire des Eyzies), Conseil Général de Dordogne, the University of Pennsylvania Museum and the National Science Foundation (Grant #BCS-1755237). V. Aldeias is funded by the European Union (ERC, MATRIX project no 101041245). Views and opinions expressed are however those of the author(s) only and do not necessarily reflect those of the European Union or the European Research Council Executive Agency. Neither the European Union nor the granting authority can be held responsible for them. Open access to this article is financed by FCT – Fundação para a Ciência e Tecnologia, within the scope of ICAREHB, program UIDP/04211/2020.

**Data availability** The micromorphological samples are curated in the Interdisciplinary Center for Archaeology and Human Behavior at University of Algarve, Portugal.

## Declarations

**Competing interests** The authors declare no competing interests.

**Open Access** This article is licensed under a Creative Commons Attribution 4.0 International License, which permits use, sharing, adaptation, distribution and reproduction in any medium or format, as long as you give appropriate credit to the original author(s) and the source, provide a link to the Creative Commons licence, and indicate if changes were made. The images or other third party material in this article are included in the article's Creative Commons licence, unless indicated otherwise in a credit line to the material. If material is not included in the article's Creative Commons licence and your intended use is not permitted by statutory regulation or exceeds the permitted use, you will need to obtain permission directly from the copyright holder. To view a copy of this licence, visit <http://creativecommons.org/licenses/by/4.0/>.

## References

- Aldeias, V., Goldberg, P., Sandgathe, D., Berna, F., Dibble, H. L., McPherron, S. P., . . . Rezek, Z. (2012). Evidence for Neandertal use of fire at Roc de Marsal (France). *Journal of Archaeological Science*, 39(7), 2414–2423. <http://www.scopus.com/inward/record.url?eid=2-s2.0-84860888706&partnerID=40&md5=a7b4aa1693589055265d813af4fa4607>
- Balzeau, A., Turq, A., Talamo, S., Daujeard, C., Guérin, G., Welker, F., . . . Lahaye, C. (2020). Pluridisciplinary evidence for burial for the La Ferrassie 8 Neandertal child. *Scientific Reports*, 10(1), 1–10.
- Benn, D. (1994). Fabric shape and the interpretation of sedimentary fabric data. *Journal of Sedimentary Research*, 64(4a), 910–915.
- Bertran, P., Caner, L., Langohr, R., Lemée, L., & d'Errico, F. (2008a). Continental palaeoenvironments during MIS 2 and 3 in southwestern France: The La Ferrassie rockshelter record. *Quaternary Science Reviews*, 27(21–22), 2048–2063. <http://www.scopus.com/inward/record.url?eid=2-s2.0-54449093275&partnerID=40>.
- Bertran, P., Caner, L., Langohr, R., Lemée, L., & d'Errico, F. (2008b). Continental palaeoenvironments during MIS 2 and 3 in southwestern France: The La Ferrassie rockshelter record. *Ninth International Conference on Luminescence and Electron Spin Resonance Dating LED99*, 27(21), 2048–2063.
- Bertran, P., Klaric, L., Lenoble, A., Masson, B., & Vallin, L. (2010). The impact of periglacial processes on Palaeolithic sites: The case of sorted patterned grounds. *Quaternary International*, 214(1–2), 17–29. <https://doi.org/10.1016/j.quaint.2009.10.021> <http://www.sciencedirect.com/science/article/B6VGS-4XM6K9J-8/2/591f9f8a3532c5860233bb474fba883>.
- Bertran, P. (2012). Dynamique sédimentaire et paléopédogenèse à La Ferrassie : Une réinterprétation. *Livret guide excursion Quaternaire Continental d'Aquitaine, excursion AFEQ, ASF*, pp. 64–77.
- Breuil, H. (1921). Communication sur les squelettes de La Ferrassie. *L'anthropologie*, 31, 342–344.
- Canti, M. G. (2017). Biospheroids produced by earthworms. In C. Nicosia & G. Stoops (Eds.), *Archaeological soil and sediment micromorphology* (pp. 47–49). Wiley-Blackwell.
- Capitan, L., & Peyrony, D. (1912). *Station préhistorique de la Ferrassie, commune de Savignac-du-Bugue (Dordogne)*. (Vol. 1). *Revue anthropologique*, pp. 29–99.

- Capitan, L., & Peyrony, D. (1909a). Deux squelettes humains au milieu de foyers de l'époque moustérienne. *Revue De L'école D'anthropologie De Paris*, 12, 402–409.
- Capitan, L., & Peyrony, D. (1909b). Deux squelettes humains au milieu de foyers de l'époque moustérienne. *Comptes Rendus Des Séances De L'académie Des Inscriptions Et Belles-Lettres*, 53(11), 797–806.
- Capitan, L., & Peyrony, D. (1911). Un nouveau squelette humain fossile. *Comptes Rendus Des Séances De L'académie Des Inscriptions Et Belles-Lettres*, 55(2), 224–227.
- Capitan, L., & Peyrony, D. (1921a). Découverte d'un sixième squelette moustérien à la Ferrassie, Dordogne. *Revue Anthropologique*, 31, 382–388.
- Capitan, L., & Peyrony, D. (1921b). Les origines de l'art à l'Aurignacien moyen: La Ferrassie. *Revue Archéologique*, 31, 92–112.
- Courty, M.-A., Goldberg, P., & Macphail, R. I. (1989). *Soils and Micromorphology in Archaeology*. Cambridge University Press.
- Delporte, H., Mazière, G., & Djindjian, F. (1977). L'Aurignacien de La Ferrassie: Observations préliminaires à la suite de fouilles récentes. *Bulletin de la Société préhistorique française. Études et travaux*, 74(Fasc. 1), 343–361.
- Delporte, H. (1984). *Le grand abri de la Ferrassie: fouilles 1968-1973* (Vol. Mémoire n° 7). Laboratoire de paléontologie humaine et de préhistoire, Université de Provence.
- Dibble, H. L., Lin, S., Sandgathe, D., & Turq, A. (2018a). Assessing the integrity of older archeological collections: An example from La Ferrassie. *Journal of Paleolithic Archaeology*, 1(3), 179–201.
- Dibble, H. L., McPherron, S. P., Goldberg P., & Sandgathe, D. (2018b). *The Middle Paleolithic Site of Pech de l'Azé IV*. Tuscaloosa, USA: Springer.
- Figueiredo, M., Fernando, A., Martins, G., Freitas, J., Judas, F., & Figueiredo, H. (2010). Effect of the calcination temperature on the composition and microstructure of hydroxyapatite derived from human and animal bone. *Ceramics International*, 36(8), 2383–2393.
- Frouin, M., Guérin, G., Lahaye, C., Mercier, N., Huot, S., Aldeias, V., Bruxelles, L., Chiotti, L., Dibble, H. L., Goldberg, P. (2017). New luminescence dating results based on polymineral fine grains from the middle and Upper Palaeolithic site of La Ferrassie (Dordogne, SW France). *Quaternary Geochronology*, 39, 131–141.
- Goldberg, P. (1992). Micromorphology, Soils, and Archaeological Sites. In V. T. Holliday (Ed.), *Soils in archaeology: Landscape evolution and human occupation* (pp. 145–168). Smithsonian Institution Press.
- Goldberg, P., & Aldeias, V. (2018). Why does (archaeological) micromorphology have such little traction in (geo)archaeology? *Archaeological and Anthropological Sciences*, 10, 269–278. <https://doi.org/10.1007/s12520-016-0353-9>
- Goldberg, P., & Berna, F. (2010). Micromorphology and context. *Quaternary International*, 214(1–2), 56–62. <https://doi.org/10.1016/j.quaint.2009.10.023> <http://www.sciencedirect.com/science/article/B6VGS-4XM6K9J-9/2/3714829a4776d30f3239b8ebc5a55bc>.
- Goldberg, P., & Macphail, R. I. (2003). Strategies and techniques in collecting micromorphology samples. *Geoarchaeology*, 18(5), 571–578. <http://www.scopus.com/scopus/inward/record.url?eid=2-s2.0-2442546685&partnerID=40&rel=R8.2.0>.
- Goldberg, P., McPherron, S. J., Dibble, H. L., & Sandgathe, D. M. (2018). Stratigraphy, deposits, and site formation. In H. L. Dibble, S. J. McPherron, P. Goldberg, & D. M. Sandgathe (Eds.), *The Middle Paleolithic Site of Pech de l'Azé IV* (pp. 21–74). Tuscaloosa, USA: Springer.
- Gómez-Olivencia, A., Crevecoeur, I., & Balzeau, A. (2015). La Ferrassie 8 Neandertal child reloaded: New remains and re-assessment of the original collection. *Journal of Human Evolution*, 82, 107–126.
- Gómez-Olivencia, A., Quam, R., Sala, N., Bardey, M., Ohman, J. C., & Balzeau, A. (2018). La Ferrassie 1: New perspectives on a “classic” Neandertal. *Journal of Human Evolution*, 117, 13–32. <https://doi.org/10.1016/j.jhevol.2017.12.004>
- Guérin, G., Frouin, M., Talamo, S., Aldeias, V., Bruxelles, L., Chiotti, L., . . . Turq, A. (2015). A multi-method luminescence dating of the Palaeolithic sequence of La Ferrassie based on new excavations adjacent to the La Ferrassie 1 and 2 skeletons. *Journal of Archaeological Science*, 58, 147–166. <https://doi.org/10.1016/j.jas.2015.01.019>
- Horwitz, L. K., & Goldberg, P. (1989). A study of Pleistocene and Holocene hyaena coprolites. *Journal of Archaeological Science*, 16(1), 71–94. [https://doi.org/10.1016/0305-4403\(89\)90057-5](https://doi.org/10.1016/0305-4403(89)90057-5)
- Jaillet, S., Sadier, B., Delannoy, J.-J., & Ployon, E. (2009). Identification de morphologies pariétales en grotte à partir d'un lever laser 3D. Application aux salles rouges de l'Aven d'Orgnac (Ardèche, France). Paper presented at the Colloque Lidar ESGT.

- Karkanas, P. (2019). Microscopic deformation structures in archaeological contexts. *Geoarchaeology*, 34(1), 15–29.
- Karkanas, P., & Goldberg, P. (2013). Micromorphology of cave sediments. In J. Shroder & A. Frumkin (Eds.), *Treatise on Geomorphology* (pp. 286–297). Academic Press.
- Karkanas, P., & Goldberg, P. (2018). *Reconstructing archaeological sites: Understanding the geoarchaeological matrix*. John Wiley & Sons.
- Karkanas, P., Bar-Yosef, O., Goldberg, P., & Weiner, S. (2000). Diagenesis in prehistoric caves: The use of minerals that form in situ to assess the completeness of the archaeological record. *Journal of Archaeological Science*, 27, 915–929.
- Karkanas, P., Rigaud, J.-P., Simek, J. F., Albert, R. M., & Weiner, S. (2002). Ash bones and guano: A study of the minerals and phytoliths in the sediments of Grotte XVI, Dordogne, France. *Journal of Archaeological Science*, 29(7), 721–732. <http://www.sciencedirect.com/science/article/pii/S0305440301907423>.
- Karnay, G., Aujoulat, N., Konik, S., Mauroux, B., Pluchery, E., & Turq, A. (1999). Notice explicative de la feuille Le Bugue à 1/50000. *Carte Géologique De La France à 1, 50000*.
- Larsen, N. K., & Piotrowski, J. A. (2003). Fabric pattern in a basal till succession and its significance for reconstructing subglacial processes. *Journal of Sedimentary Research*, 73(5), 725–734.
- Lauritzen S. E., & Lundberg J. (2000). Solutional and erosional morphology. In A. B. Kimchouk, Ford, D. C., Palmer, A. N., & Dreybrodt, W. (Eds.), *Speleogenesis, evolution of karst aquifers* (pp. 408–426). National Speleological Society Editions.
- Laville, D. (2007a). La Ferrassie: Taphonomie d'un site Sépulcral Moustérien (Mémoire de Master). *Université de Liège*, 2 volumes, p. 118.
- Laville, D. (2007b). Les monticules de La Ferrassie: Entre réalité géologique et vue de l'esprit. *Bulletin De La Société Historique Et Archéologique Du Périgord*, 134(4), 507–522.
- Laville, H., & Tuffreau, A. (1984). Les dépôts du grand abri de la Ferrassie: Stratigraphie, signification climatique et chronologie. *Le Grand Abri De La Ferrassie, Fouilles, 1968–1973*, 22–50.
- Lenoble, A., & Bertran, P. (2004). Fabric of Palaeolithic levels: Methods and implications for site formation processes. *Journal of Archaeological Science*, 31(8), 457–469. <http://www.scopus.com/inward/record.url?eid=2-s2.0-3042636770&partnerID=40>.
- Macphail, R. I., & Goldberg, P. (2017). *Applied soils and micromorphology in archaeology*. Cambridge University Press.
- Mallol, C., Hernández, C. M., Cabanes, D., Sistiaga, A., Machado, J., Rodríguez, Á., . . . Galván, B. (2013). The black layer of Middle Palaeolithic combustion structures. Interpretation and archaeostratigraphic implications. *Journal of Archaeological Science*, 40(5), 2515–2537. <https://doi.org/10.1016/j.jas.2012.09.017>
- Masson, B. (2010). Combustion features and periglacial structures: A new taphonomic analysis of Mousterian combustion features at Saint-Vaast-la-Hougue (50). *P@lethnologie*, 2010(2), 5–23.
- McPherron, S. (2005). Artifact orientations and site formation processes from total station proveniences. *Journal of Archaeological Science*, 32, 1003–1014.
- McPherron, S. P. (2018). Additional statistical and graphical methods for analyzing site formation processes using artifact orientations. *PLoS one*, 13(1), e0190195. <https://doi.org/10.1371/journal.pone.0190195>
- Nicosia, C., & Stoops, G. (2017). *Archaeological soil and sediment micromorphology*. Wiley-Blackwell.
- Palmer, A. N. (2007). *Cave Geology*. Cave Books Editions, p. 454.
- Peyrony, D. (1934). *La Ferrassie. Moustérien, Périgordien, Aurignacien*. Paris: Editions Leroux.
- Renault, P. (1968). *Contribution à l'étude des actions mécaniques et sédimentologiques dans la spéléogénèse* (A. d. Spéléologie Ed. Vol. 22): Imprimerie M. Declume.
- Rowley, T., Giardino, J. R., Granados-Aguilar, R., & Vitek, J. D. (2015). Chapter 13 - Periglacial processes and landforms in the critical zone. In J. R. Giardino & C. Houser (Eds.), *Developments in earth surface processes* (Vol. 19, pp. 397–447). Elsevier. <https://doi.org/10.1016/B978-0-444-63369-9.00013-6>
- Shahack-Gross, R., Berna, F., Karkanas, P., Lemorini, C., Gopher, A., & Barkai, R. (2014). *Journal of Archaeological Science*, 44, 12–21. <http://www.sciencedirect.com/science/article/pii/S0305440313004068>.
- Slabe, T. (1995). *Cave rocky relief and its speleogenetical significance*. Založba ZRC.
- Stiner, M. C., Kuhn, S. L., Weiner, S., & Bar-Yosef, O. (1995). Differential burning, recrystallization, and fragmentation of archaeological bone. *Journal of Archaeological Science*, 22(2), 223–237. <http://www.scopus.com/inward/record.url?eid=2-s2.0-0000157557&partnerID=40&md5=91b053a5e1ef67cda8381315182380dd>.
- Stoops, G. (2021). *Guidelines for analysis and description of soil and regolith thin sections* (2nd ed.). Wiley.

- Stoops, G., Marcelino, V., & Mees, F. (Eds.). (2010). *Interpretation of micromorphological features of soils and regoliths*. Elsevier.
- Stoops, G., Marcelino, V., & Mees, F. (2018). *Interpretation of micromorphological features of soils and regoliths*. Elsevier.
- Talamo, S., Aldeias, V., Goldberg, P., Chiotti, L., Dibble, H. L., Guérin, G., . . . McPherron, S. J. P. (2020). The new 14C chronology for the Palaeolithic site of La Ferrassie, France: The disappearance of Neanderthals and the arrival of Homo sapiens in France. *Journal of Quaternary Science*, 35(7), 961–973. <https://doi.org/10.1002/jqs.3236>
- Texier, J.-P. (2006). La Ferrassie. In J.-P. Texier, B. Kervazo, A. Lenoble, & R. Nespoulet (Eds.), *Sédimentogenèse de Sites Préhistoriques Classiques du Périgord, Édition Numérique I 2006* (pp. 23–30). Pôle International de la Préhistoire.
- Texier, J.-P., Agsous, S., Kervazo, B., Lenoble, A., & Nespoulet, R. (2006). *Sédimentogenèse de sites préhistoriques classiques du Périgord*. Les Eyzies: Pole International de la Préhistoire.
- Texier, J.-P. (2009). *Histoire géologique de sites préhistoriques classiques du Périgord: une vision actualisée: La Micoque, la grotte Vauffrey, Le Pech de l'Azé I et II, La Ferrassie, l'abri Castenet, Le Flageolet, Laugerie haute* (Vol. 25). Paris: Éditions du Comité des travaux historiques et scientifiques.
- Thompson, T. J. U., Gauthier, M., & Islam, M. (2009). The application of a new method of Fourier transform infrared spectroscopy to the analysis of burned bone. *Journal of Archaeological Science*, 36(3), 910–914. <http://www.scopus.com/scopus/inward/record.url?eid=2-s2.0-58149293411&partnerID=40>.
- Turq, A., Dibble, H. L., McPherron, S., Sandgathe, D., Mercier, N., Bruxelles, L., . . . Madelaine, S. (2012). Reprise des fouilles dans la partie ouest du gisement de la Ferrassie, Savignac-de-Miremont, Dordogne : problématique et premiers résultats. *Quaternaire Continental d'Aquitaine. excursion AFEQ*, 78–87.
- Van Vliet-Lanoë, B. (1991). Differential frost heave, load casting and convection: Converging mechanisms; a discussion of the origin of cryoturbations. *Permafrost and Periglacial Processes*, 2(2), 123–139.
- Weiner, S. (2010). *Microarchaeology beyond the visible archaeological record*.
- Weiner, S., Goldberg, P., & Bar-Yosef, O. (2002). Three-dimensional distribution of minerals in the sediments of Hayonim Cave, Israel: Diagenetic processes and archaeological implications. *Journal of Archaeological Science*, 29, 1289–1308.
- Weiner, S., Berna, F., Cohen-Ofri, I., Shahack-Gross, R., Albert, R. M., Karkanas, P., . . . Bar-Yosef, O. (2007). Mineral distributions in Kebara Cave: Diagenesis and its effect on the archaeological record. In O. Bar-Yosef & L. Meignen (Eds.), *Kebara Cave, Mt. Carmel, Israel: The Middle and Upper Paleolithic Archaeology* (pp. 131–146). American School of Prehistoric Research Bulletin 49, Peabody Museum of Archaeology and Ethnology, Harvard University.

**Publisher's Note** Springer Nature remains neutral with regard to jurisdictional claims in published maps and institutional affiliations.

## Authors and Affiliations

Vera Aldeias<sup>1</sup> · Dennis Sandgathe<sup>2</sup> · Shannon J. P. McPherron<sup>1,3</sup> ·  
Laurent Bruxelles<sup>4</sup> · Alain Turq<sup>5,6</sup> · Paul Goldberg<sup>1,2,7,8</sup>

✉ Vera Aldeias  
valdeias@ualg.pt

<sup>1</sup> Interdisciplinary Center for Archaeology and the Evolution of Human Behavior (ICArEHB),  
University of Algarve, Campus Gambelas, 8005-139 Faro, Portugal

<sup>2</sup> Department of Archaeology, Simon Fraser University, 8888 University Drive, Burnaby,  
BC V5A-1S6, Canada

<sup>3</sup> Department of Human Origins, Max Planck Institute for Evolutionary Anthropology, Deutscher  
Platz 6, 04103 Leipzig, Germany

<sup>4</sup> Traces Laboratory, CNRS, Toulouse University, Toulouse, France

<sup>5</sup> Musée de SauveTerre, 51 rue du vieux bourg, 47500 Sauveterre-la-Lémance, France

<sup>6</sup> PACEA, UMR 5199, Université de Bordeaux, CNRS, Avenue Des Facultés, Talence Cedex,  
33405 Bordeaux, France

<sup>7</sup> Geoarchäologie Institut Für Naturwissenschaftliche Archäologie (INA),  
Eberhard-Karls-Universität Tübingen, Hölderlinstr. 12, 72074 Tübingen, Germany

<sup>8</sup> SEALS, University of Wollongong, Northfields Ave. Wollongong, Wollongong, NSW 2522,  
Australia



## Terms and Conditions

Springer Nature journal content, brought to you courtesy of Springer Nature Customer Service Center GmbH (“Springer Nature”).

Springer Nature supports a reasonable amount of sharing of research papers by authors, subscribers and authorised users (“Users”), for small-scale personal, non-commercial use provided that all copyright, trade and service marks and other proprietary notices are maintained. By accessing, sharing, receiving or otherwise using the Springer Nature journal content you agree to these terms of use (“Terms”). For these purposes, Springer Nature considers academic use (by researchers and students) to be non-commercial.

These Terms are supplementary and will apply in addition to any applicable website terms and conditions, a relevant site licence or a personal subscription. These Terms will prevail over any conflict or ambiguity with regards to the relevant terms, a site licence or a personal subscription (to the extent of the conflict or ambiguity only). For Creative Commons-licensed articles, the terms of the Creative Commons license used will apply.

We collect and use personal data to provide access to the Springer Nature journal content. We may also use these personal data internally within ResearchGate and Springer Nature and as agreed share it, in an anonymised way, for purposes of tracking, analysis and reporting. We will not otherwise disclose your personal data outside the ResearchGate or the Springer Nature group of companies unless we have your permission as detailed in the Privacy Policy.

While Users may use the Springer Nature journal content for small scale, personal non-commercial use, it is important to note that Users may not:

1. use such content for the purpose of providing other users with access on a regular or large scale basis or as a means to circumvent access control;
2. use such content where to do so would be considered a criminal or statutory offence in any jurisdiction, or gives rise to civil liability, or is otherwise unlawful;
3. falsely or misleadingly imply or suggest endorsement, approval, sponsorship, or association unless explicitly agreed to by Springer Nature in writing;
4. use bots or other automated methods to access the content or redirect messages
5. override any security feature or exclusionary protocol; or
6. share the content in order to create substitute for Springer Nature products or services or a systematic database of Springer Nature journal content.

In line with the restriction against commercial use, Springer Nature does not permit the creation of a product or service that creates revenue, royalties, rent or income from our content or its inclusion as part of a paid for service or for other commercial gain. Springer Nature journal content cannot be used for inter-library loans and librarians may not upload Springer Nature journal content on a large scale into their, or any other, institutional repository.

These terms of use are reviewed regularly and may be amended at any time. Springer Nature is not obligated to publish any information or content on this website and may remove it or features or functionality at our sole discretion, at any time with or without notice. Springer Nature may revoke this licence to you at any time and remove access to any copies of the Springer Nature journal content which have been saved.

To the fullest extent permitted by law, Springer Nature makes no warranties, representations or guarantees to Users, either express or implied with respect to the Springer nature journal content and all parties disclaim and waive any implied warranties or warranties imposed by law, including merchantability or fitness for any particular purpose.

Please note that these rights do not automatically extend to content, data or other material published by Springer Nature that may be licensed from third parties.

If you would like to use or distribute our Springer Nature journal content to a wider audience or on a regular basis or in any other manner not expressly permitted by these Terms, please contact Springer Nature at

[onlineservice@springernature.com](mailto:onlineservice@springernature.com)